PHILOSOPHICAL TRANSACTIONS OF THE ROYAL SOCIETY A MATHEMATICAL, PHYSICAL & ENGINEERING SCIENCES

Photoelectron Spectroscopy: Retrospects and Prospects

K. Siegbahn

Phil. Trans. R. Soc. Lond. A 1986 **318**, 3-36
doi: 10.1098/rsta.1986.0057

Phil. Trans. R. Soc. Lond. A **318**, 3–36 (1986)

Printed in Great Britain

Photoelectron spectroscopy: retrospects and prospects

By K. Siegbahn

Department of Physics, University of Uppsala, Box 530, *S*-751 21 *Uppsala, Sweden*

Electron spectroscopy is at present developing towards higher resolution both at low and high energies of the exciting radiation. The limitations are set by quite different reasons in the two regions, i.e. in the v.u.v. and in the X-ray region. In the former region the limit is due to several independent factors: Doppler broadening in the sample gas, small residual electric fields over the sample volume and, of course, possible imperfections of the electron spectrometer. In addition to this the ultimate resolution is set by the inherent linewidth of the u.v. radiation. This width is dependent on the extremely high temperature of the light-source gas, owing to Doppler effect, and the gas pressure, owing to self-absorption. If a resolution of 5 meV should be attained all these factors have to be thoroughly studied and separately handled. This leads to arrangements where supersonic molecular jet beams are required, where developments of specially designed light sources are necessary and where extreme care has to be taken over the details of the spectrometer.

A new extension of electron spectroscopy is under development. It consists of a simultaneous excitation or fragmentation of the molecules at photoionization. There are several ways to arrange such a spectroscopy, which, for convenience, could be classified as a 'dynamic' electron spectroscopy in contrast to the usual 'static' spectroscopy, which deals with the emission of electrons from normal molecules. A particularly attractive scheme for such a dynamic spectroscopy would be a combination between electron and laser spectroscopy.

In the X-ray region high resolution cannot be attained unless the selected X-rays are further properly monochromatized towards the limit set by the rocking curve of the diffracting crystal being used. To secure sufficiently high intensity a high-power X-ray source has to be used, either a synchrotron source or a water-cooled, swiftly rotating anode. For the latter, experiments and calculations show that Al Kα and spherically bent quartz crystals ($10\bar{1}0$, 1st order diffraction) with almost backwards reflection can yield a resolution of 0.15 eV. With nearly identical geometry Ag Lα (second order) has a rocking curve of the same crystal, which amounts to 0.08 eV. Sc K$\beta_{1,3}$ and Ti Kα (third order) have 0.03 eV resolution, and Mn Kα and Cr K$\beta_{1,3}$ (fourth order) also 0.03 eV. For most purposes the first choice (Al Kα) is the one to be preferred.

Some recent investigations related to solids, gases and liquids made by several groups in our laboratory are reviewed.

1. Introduction

Although photoelectron spectroscopy traces several of its fundamentals from studies made a very long time ago it must still be regarded as a new spectroscopy far from its ultimate shape. One can easily forecast many important developments to be made in the future concerning both spectral and spatial resolution and also improvements in convenience of handling samples of different kinds. Gradually these advances will result in an appreciable widening of the scope of this spectroscopy, enabling new scientific lines of research. In this contribution to the report

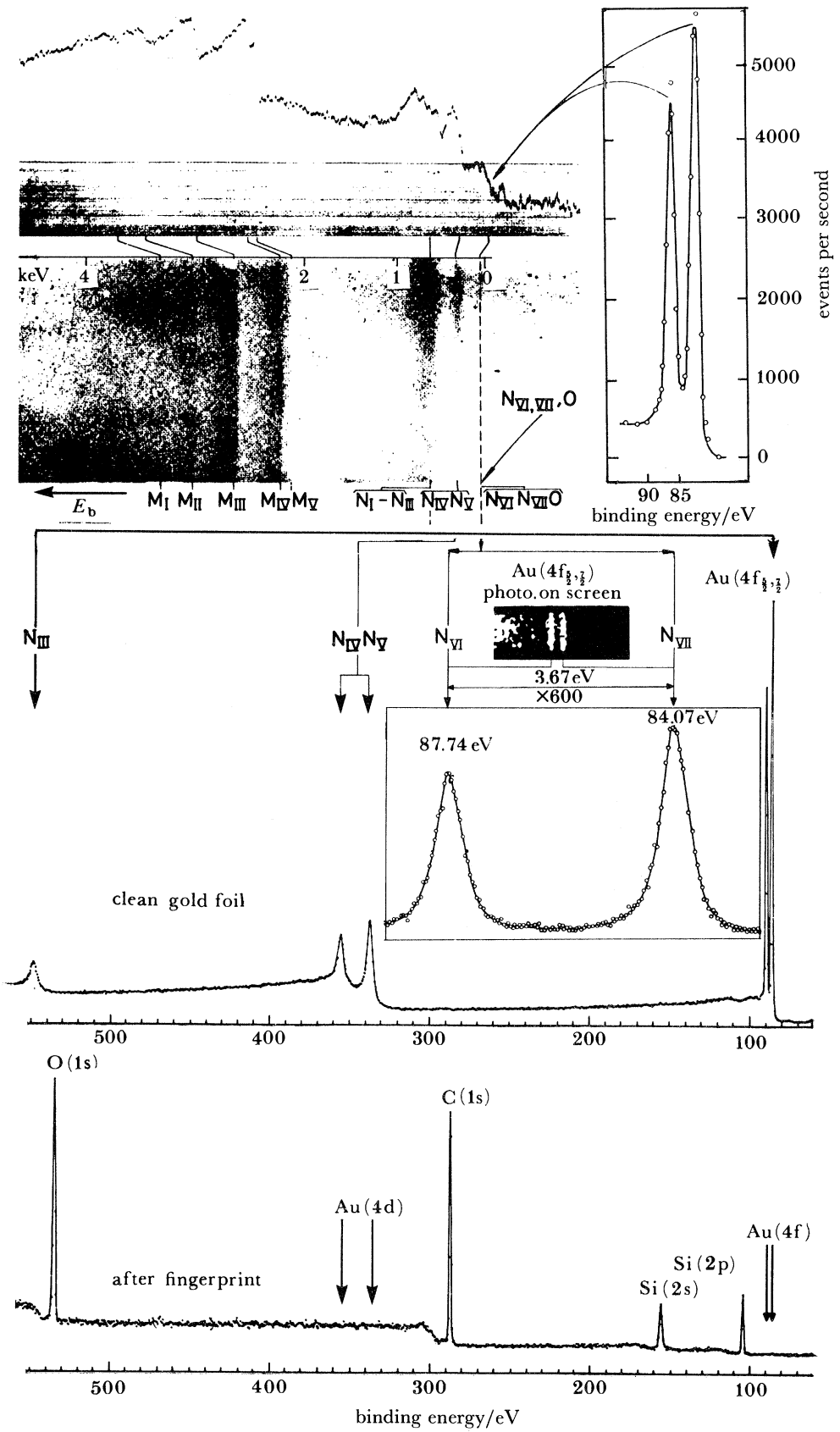

FIGURE 1. For description see opposite.

of a Royal Society Discussion Meeting, it is appropriate for me to start my review by recalling the prominent role that has been played by British scientists not only in recent times, but also in the early history of this field. I am particularly referring to the work by H. Robinson (1925), who was able to establish that electrons expelled from metals by means of the photoelectric effect exhibited an energy distribution that was consistent with the shell structure of matter. He and other scientists from this period were able to deduce approximate values of atomic energies from inspection of their photographic plates. During the thirties and forties much of the interest in atomic physics shifted to nuclear physics. Partly because of this and partly owing to the lack of adequate methods for handling the experimental problems associated with electron spectroscopy, the field had to wait for its development and exploration until the 1950s. Also, in this later period British scientists have made essential contributions and several of those concerned attended this meeting (for example, D. Turner (Turner *et al.* 1970) and W. Price (Price & Turner 1970).

The early period is represented by the top of figure 1, which shows a photographic recording of the photoelectron spectrum of gold by Robinson in 1925. The various levels in gold are distinguished well in Robinson's spectrum and also in the corresponding photometric recording. The well known $N_{VI, VII}$ doublet, extensively used for calibrations in modern electron spectroscopy, is not observed in this early spectrum, however, and obviously the distributions look rather more like X-ray absorption edges than true lines.

At the end of the fifties line spectra were achieved, however, from solid materials at high resolution with widths approaching the inherent widths of atomic levels. The state of the art during this later period (Siegbahn *et al.* 1967, 1969) is illustrated by the recordings of the gold spin doublet made around 1965 (to the right of Robinson's spectrum). The same spectrum taken some years later is shown in the middle of the figure on an energy scale expanded by a factor 600 compared to Robinson's spectrum. The improvement in resolution between the two later spectra is due to the introduction of monochromatization by means of crystal diffraction of the Al Kα radiation (Siegbahn *et al.* 1972; Gelius & Siegbahn 1972). This made it possible to pass beyond the previous limit set by the inherent width of this radiation.

The lowest part of the figure illustrates one particularly important feature of electron spectroscopy with direct bearing upon the title of this meeting: Studies of *surfaces* of solids by electron spectroscopy. The difference between the middle and the lowest part of the figure demonstrates the *surface sensitivity* of this spectroscopy. A fingerprint on the gold foil completely wipes out the gold lines and replaces them by other lines dependent on what elements happened to be on the surface layer of that finger. This property of electron spectroscopy we found most disturbing to begin with and not until we had learnt how to deal with it did we gradually realize that this feature actually contained one of the most rewarding aspects of the whole spectroscopy.

FIGURE 1. Electron spectra of gold. Upper left: spectrum photographically recorded by Robinson in 1925. Upper right: spectrum recorded around 1965 by using non-monochromatized Mg Kα excitation. The N_{VI}, N_{VII} levels are seen as two well resolved lines in this spectrum, visible in the earlier photometric recording as a hump of unresolved levels N_{VI}, N_{VII} and O. Middle: spectrum recorded after 1972 by monochromatized Al Kα excitation. The magnification of this spectrum is 600 times that of Robinson's photographic recording. The binding energy is *ca.* 85 eV, the retardation 1100 V and the kinetic energy 300 eV. Lower part: spectrum of the gold foil with a fingerprint on the surface. The electron lines are entirely due to the fingerprint and the gold lines are missing.

PHILOSOPHICAL TRANSACTIONS OF THE ROYAL SOCIETY A MATHEMATICAL, PHYSICAL & ENGINEERING SCIENCES

Another feature that we did not appreciate either in the beginning was the *chemical* dependence of the line positions. We started out as atomic physicists and were looking for regularities of binding energies when going from one element to the other, in a similar way to Moseley's diagrams in X-ray spectra. However, such regularities were heavily disturbed when we used elements in different chemical compounds, for example a metal or a metal oxide. Again, after some time we realized that this was another feature of the spectroscopy that should be important, not least in surface science when materials start to corrode or, in general, in the characterization of the chemical composition of surfaces.

2. Surface sensitivity

I now illustrate the surface sensitivity with a more recent example. The lower part of figure 2 shows a spectrum of a silicon surface (Maripuu 1983). One observes two main peaks due to Si(2s) and Si(2p). One also distinguishes two satellites following each main line, which are due to energy losses, characteristic of the material. Closer to the main line one can also notice an extra line with low intensity. This line emanates from the surface layer, and is chemically shifted due to oxidation. In the upper part of figure 2 this surface chemical effect has been enhanced simply by tilting the surface relative to the direction of the electron emission from 63° to 13°. This increases the distance an electron emitted at a certain depth has to travel

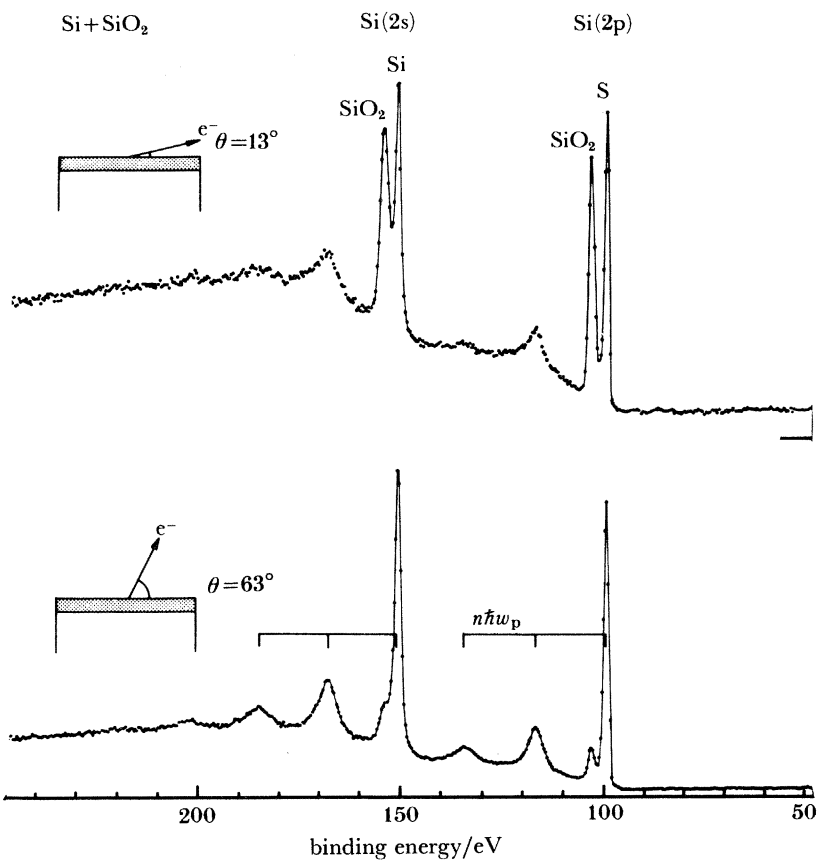

Figure 2. Spectrum of a slightly oxidized silicon surface. By tilting the crystal the oxide surface layer is emphasized.

through the material before it reaches the surface, and consequently suppresses the intensity from the bulk. This simple procedure to get a preliminary depth scan of a sample is most powerful and can, for example, immediately tell if a certain line is due to the surface or to the bulk.

The limit of the surface sensitivity is hard to set. It depends on many factors, for example the background. Values around 10^{-3} of one single atomic layer were reported some years ago. This figure can probably be further improved presently.

3. Resolution and background

To distinguish various structures in electron spectroscopy the *resolution* is of particular importance. Often chemical shifts are small and in many cases one also has to rely on deconvolution of composite line structures. Even small improvements in the resolution can have a decisive influence on the possibilities of resolving a certain line structure. High intensity is a prerequisite for reliable deconvolution, and a low background greatly improves the possibility of observing features with low intensity in the spectrum. The higher the resolution and the smaller the linewidths the more the background can be suppressed.

If we pass from figure 2 to figure 3 we observe that the latter spectrum again exhibits the Si spectrum from a single crystal, but taken at a much improved resolution (Gelius *et al.* 1984). The unresolved Si(2p) line of figure 2 is, in figure 3, well resolved into its two spin components

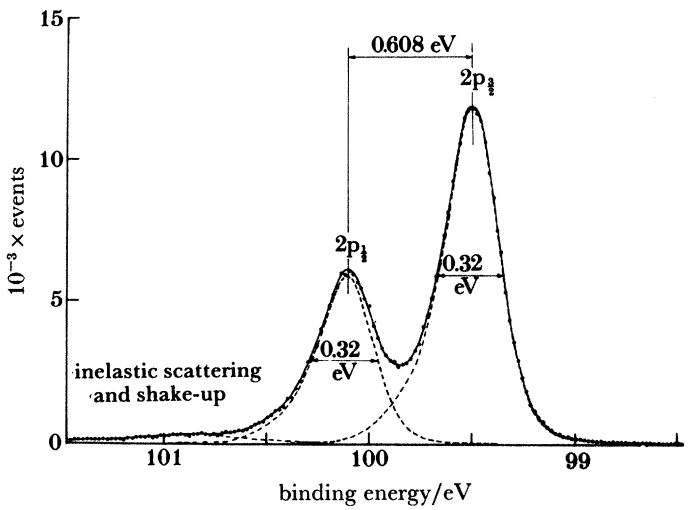

Figure 3. Resolved $2p_{\frac{1}{2}}$ and $2p_{\frac{3}{2}}$ core lines of Si(111) for $T = 300$ K and $\theta = 45°$. Observe the low background.

$2p_{\frac{1}{2}}$ and $2p_{\frac{3}{2}}$. This spectrum can be analysed in considerable detail. An analysis of the right side of the Si($2p_{\frac{3}{2}}$) line shows that it is perfectly described by a Voigt function corresponding to the convolution of a Lorentzian with a f.w.h.m. of 0.08 eV and a Gaussian with a f.w.h.m. of 0.255 eV. In an experiment on gaseous CH_4 with the same high resolution (see figure 4) we were able to resolve the different core vibrational components of C(1s) (a vibration set up due to a shrinkage of 0.05 Å† at the core ionization). Under these circumstances we could more

† 1 Å = 10^{-10} m = 0.1 nm.

precisely check the spectrometer function, which is a slightly skew Gaussian with a f.w.h.m. less than 0.25 eV. Combined with a similar analysis of the Pt valence band we arrive at a spectrometer function that can be described well by a single Gaussian function with a f.w.h.m. of 0.21 eV. The difference in Gaussian width between 0.21 eV and the 0.255 eV found in the Si($2p_{\frac{3}{2}}$) analysis can be explained by a phonon broadening of about 0.14 eV. This phonon

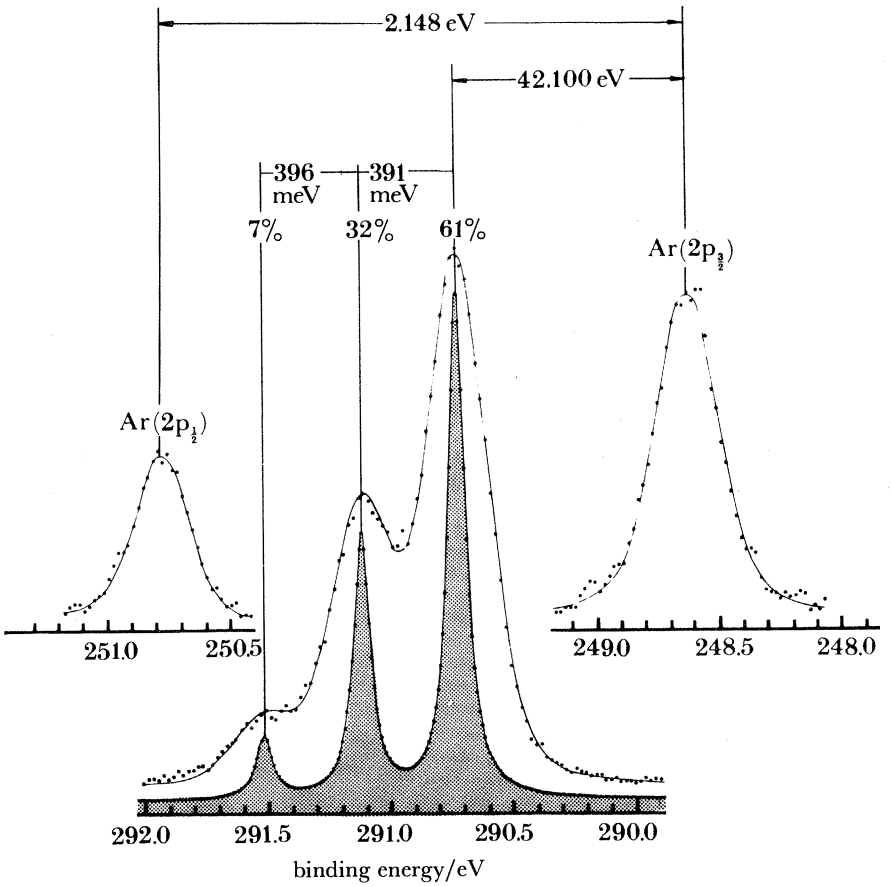

FIGURE 4. Core vibrational components of C(1s) of gaseous methane taken at high resolution. Argon lines are simultaneously recorded for calibration.

broadening is likely to be caused by the photoionization of a localized core electron in analogy with the vibrational excitation demonstrated for methane. The remarkably low background, essentially zero, in figure 3 should be observed. As mentioned, such a low background facilitates the observation and interpretation of weak structures. For the present case the weak low-energy component is attributed to inelastic scattering with some contribution from a shake-up structure. This explanation is consistent with the known band gap of Si, which is 1.1 eV. An alternative explanation could be to attribute this structure to a submonolayer of SiO_x, which would give rise to a Si(2p) line with a chemical shift of 1.4 eV. However, this explanation can be rejected in the present case after a study of the Si(2p) line under grazing angle, according to the procedure outlined in figure 2. This tilt experiment gave as a result that a weak carbon line due to a very small submonolayer of carbon (which is often a small natural component

on many surfaces even at ultra-high vacuum conditions) was enhanced by a factor of 10 without changing the intensity around 101 eV relative to the Si(2p) line. Therefore this structure must be attributed to bulk phenomena.

4. The post-collision interaction

High resolution is the prerequisite for decomposing a complex line structure. At sufficiently high resolution even the shape of a single line can be examined in detail and analysed in terms of the dynamics of the electron emission process. One example is the post collision interaction (p.c.i.), which can be observed when the emitted electron feels a changing potential when leaving the atom.

Figure 5 shows the Auger electron spectrum of argon (Helenelund 1984) in the régime for LMM emission with electrons of two different energies for excitation. At sufficiently small excess energy above threshold the lines shift their positions and furthermore, the shapes of the lines start to become asymmetric with a sharpening of the edge on the low-energy side. This sharpening can be so pronounced that it (incorrectly) seems to be in conflict with the uncertainty principle relating the linewidth to the actual lifetime of the hole state. The steep slope of the line on the left side in figure 6 taken at very high resolution corresponds to an excessively long lifetime. All these findings can, however, be explained in the following way. Near threshold the incoming electron looses almost all of its kinetic energy when expelling an L electron into the continuum. This electron will then also have a very small kinetic energy

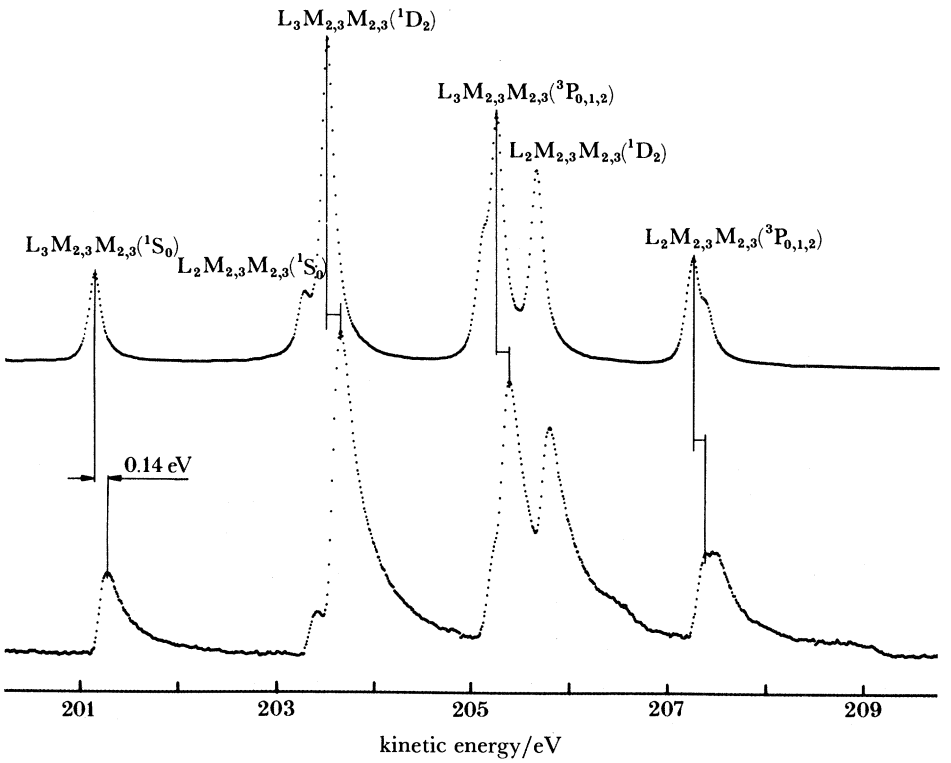

Figure 5. Argon $L_{2,3}M_{2,3}M_{2,3}$ Auger electron spectra, excited by means of electrons at two different excess energies (2750 eV for top spectrum and 30 eV for bottom) above threshold. The shifts and asymmetries of the lines are caused by the post-collision interaction (p.c.i.) effect.

and both these electrons will therefore still be close to the atom when the hole state decays by emitting a fast Auger electron. This electron, which is recorded in the spectrum, will feel a potential, which to a variable extent is screened by the two slow electrons. The longer the lifetime of the hole state, the further away from the atom will the two screening electrons be when the Auger electron is emitted and, consequently, the less will the p.c.i. screening effect be. The screening will in general result in a shift of the line position in a direction towards lower binding energies. Furthermore, a decay event occurring after a relatively short time will result in an Auger electron feeling the full p.c.i. effect, which consequently will be displaced far away towards the right side of the line. The reverse will occur for late events. The net result of all these events is a distorted electron line shape corresponding to the final dispersion of the hole state on a timescale of around 10^{-15} s. The recorded line shape can be compared to that quantum theoretically calculated under some very reasonable assumptions and the result is shown in figure 6. The shift of the line and its shape fit perfectly to the picture of p.c.i. given here. Some additional line structures with low intensity appear at low excitation energies. These can be explained as due to low-energy electron transitions to bound Rydberg states in a 'shake-down' process.

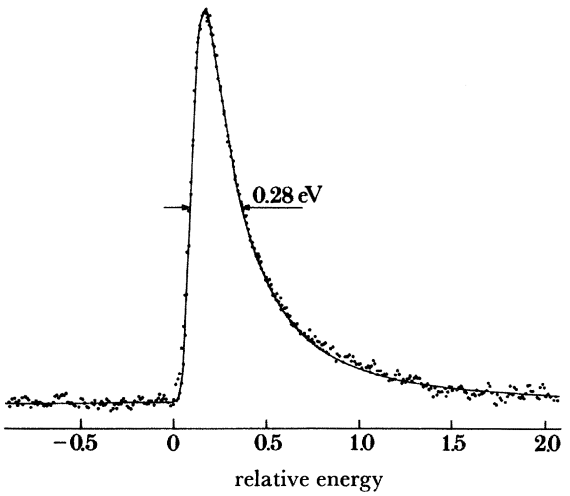

FIGURE 6. Comparison between the theoretical and experimental line shapes in p.c.i. as obtained in the spectrum of figure 5.

Recently, our group recorded a first example of the similar p.c.i. effect occurring at the excitation by means of X-ray photons instead of electrons (see figure 7). The selected case was Se, which happens to have a $2p_{\frac{3}{2}}$ binding energy of 1442 eV, which is close to the exciting Al Kα line at 1487 eV. The emitted $2p_{\frac{3}{2}}$ photoelectrons from Se have consequently a sufficiently low kinetic energy (45 eV) to screen the atomic potential at the subsequent emission of the LMM Auger electrons. Thus the Auger line is subject to the p.c.i. effect, i.e. it has an asymmetric line shape and a shift. Not unexpectedly, the simultaneously recorded Se($2p_{\frac{3}{2}}$) photoline exhibited the mirror effect, since the total energy available at the emission of the two electrons, the photoelectron and the Auger electron, is shared between them.

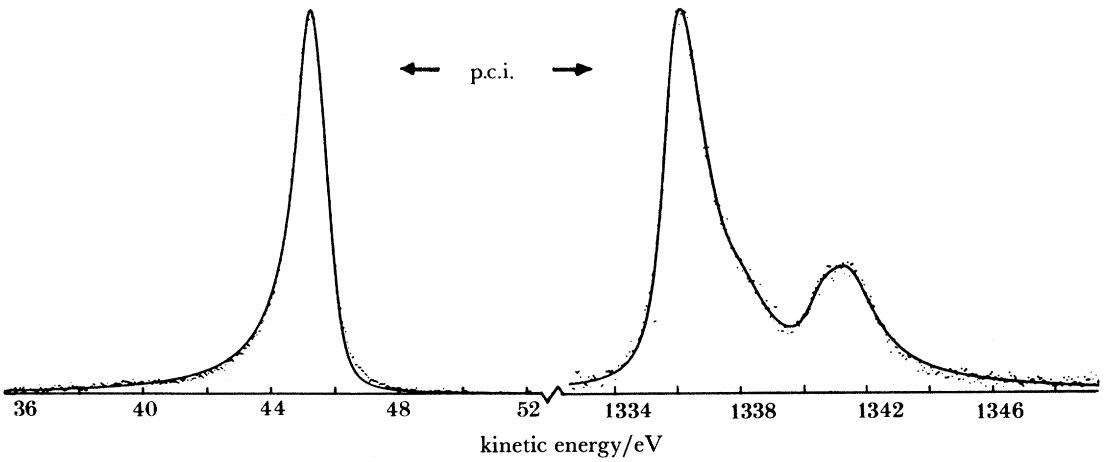

FIGURE 7. P.c.i. effect as observed for selenium photo- and Auger electron lines by means of Al Kα photon excitation.

5. SURFACE–BULK PROPERTIES AND REFERENCE LEVELS

The experimental accuracy in the determination of photoelectron or Auger electron peak positions have gradually improved to such an extent that the binding energies that can be extracted from electron spectra in principle can be given with errors in the 0.1 eV range and even much less (*ca.* 1 meV) for gases. It is then of importance to carefully consider problems related to the choice of reference levels to connect electron spectroscopic data with other data. Core electron binding energies for a metal are measured relative to the Fermi level. To transfer this binding energy to that referred to the vacuum level of the free atoms, one should add a metallic work function ϕ.

One can also proceed by means of a thermochemical approach. One then assumes a complete screening of the positive hole left behind in the metal lattice at the photoelectron emission due to the good mobility of the conduction electrons. This is a generally accepted assumption in electron spectroscopy to treat the relaxation in metals. The 'equivalent core' model is extensively used in electron spectroscopy. It states that the core-ionized atom is treated as an impurity atom with nuclear charge $Z+1$. With these assumptions a Born–Haber cycle can be performed (Johansson & Mårtensson 1980) that connects the binding energy shift ΔE_{C} to macroscopically measurable quantities like the cohesive energies and solution energies in metals. ΔE_{C} is the shift between the metal core level referred to the Fermi level $E^{\mathrm{m}}_{\mathrm{C,F}}$ and the corresponding free atom referred to the vacuum level $E^{\mathrm{a}}_{\mathrm{C}}$ according to (see figure 8)

$$\Delta E_{\mathrm{C}} = E^{\mathrm{a}}_{\mathrm{C}} - E^{\mathrm{m}}_{\mathrm{C,F}}.$$

The Born–Haber cycle gives the relation

$$\Delta E_{\mathrm{C}} = I^{Z+1}_{(Z)} + E^{Z+1}_{\mathrm{coh}} - E^{Z}_{\mathrm{coh}} - E^{\mathrm{imp}}_{Z+1}(Z).$$

Here m denotes the metal, a the atom, C the core, F the Fermi level, Z the atomic number and I the appropriate valence ionization energy (usually the first ionization energy). E_{coh} is the cohesive energy and $E^{\mathrm{imp}}_{Z+1}(Z)$ is the solution energy of impurity atom $Z+1$ in metal Z.

The dominating contributions to the shifts are the difference in cohesive energy between the $Z+1$ and Z metal and the ionization energy of the $Z+1$ atom.

The same treatment as for metallic bulk can also be applied to surface core-level shifts. The surface atoms experience a different potential compared to the layers below because of the lower coordination number. This results in somewhat different core-level binding energies. One can extend the previous Born–Haber cycle model to account for the surface–bulk core-level shift.

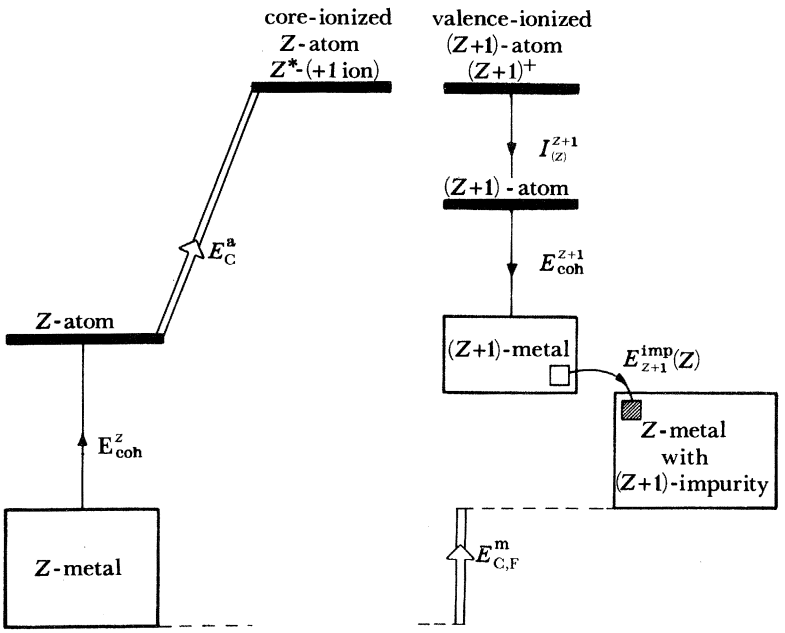

FIGURE 8. Born–Haber cycle for a metal, connecting the binding-energy shift between a metal core level referred to the Fermi level and the corresponding free atom referred to the vacuum level.

Empirically, the surface cohesive energy is approximately 80% of the bulk value. The result is then

$$\Delta E_C^{s,b} = E_C^s - E_C^b = 0.2\,(E_{coh}^{Z+1} - E_{coh}^{Z} - E_{Z+1}^{imp}(Z)).$$

This equation obviously relates the surface chemical shift and the heat of surface segregation of a $Z+1$ substitutional impurity in the Z metal.

In certain cases the shift between the surface layer and the bulk can be so large that two different, well separated lines appear in the electron spectrum at sufficiently high resolution, one originating from the surface, the other from the bulk. Figure 9 is a recent example of this (Nilsson *et al.* 1985). It shows core level shifts of the 4f levels in ytterbium by using He(II) radiation. Also the 5p levels experience the same shifts. The measured shifts agree well with calculated data for the segregation of Yb(III) impurity atoms.

Often in surface science not only the top layer but also the composition and the chemical bonds between atoms *close to and below* the top surface layer are of importance. When some element has a concentration profile within the electron escape depth, i.e. when there are surface layers of different composition with a thickness less than the escape depth, the peak amplitude of that element shows a dependence on the exit angle. The surface concentration profile, in accordance with the previous example of figure 2, can then be investigated.

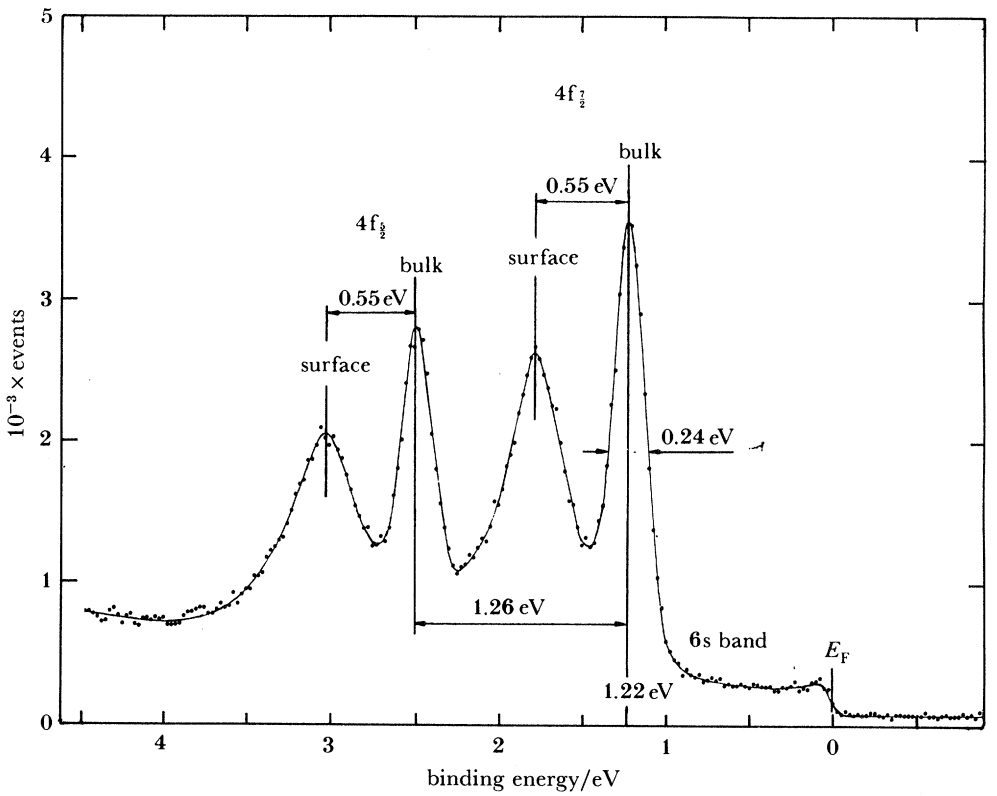

FIGURE 9. Core-level shifts between surface and bulk of the 4f levels in ytterbium at 300 K and for $L\nu = 40.81$ eV.

Such a study of medical interest dealt with blood-compatible surfaces (Lindberg *et al.* 1982). The systems studied were colloidal heparin, or dextran sulphate stabilized with hexadecyl ammonium chloride, deposited onto steel substrates, and chemically related substances. By using the angular dependence techniques, it was then found that the intensity ratio for the S(2p) peaks from disulphide and sulphate exhibit angular dependence for albumin-covered heparin-glutar and dextran sulphate-glutar surfaces, which indicate that the disulphide groups are positioned closer to the external surface than the sulphate groups.

In a series of experiments (Larsson *et al.* 1982) on a similar problem cationic polyethyleneimine was adsorbed on sulphated polyethylene surfaces at different pH, varying from 4.0 to 9.0. From the angular dependence of the amine: protonated-amine peak ratio (see figure 10*a*) it was possible to conclude that there was an accumulation of charged amine groups towards the sulphate surface at high pH. The angular dependence of the intensity ratio $I(\mathrm{N})/I(\mathrm{N}^+)$ (neutral amine: protonated amine) furthermore shows that adsorption at pH 4.0 gives a higher relative amount of charged groups and that this amount is independent of the exit angle. Adsorption at pH 9.0 gives a relatively larger amount of neutral amine groups and a $I(\mathrm{N})/I(\mathrm{N}^+)$ ratio that is dependent on the exit angle. A straightforward interpretation of these results is that the configuration of PEI when adsorbed at pH 4 is essentially flat on the surface while adsorption at pH 9.0 gives a 'layered' configuration with the charged groups (N^+) closer to the sulphated surface and the neutral groups further out according to the figure 10*b*. The fact that the number of charged amino groups remains constant leads to the conclusion that the adsorption could be considered as an ion exchange reaction. The results also imply that polymer surfaces with

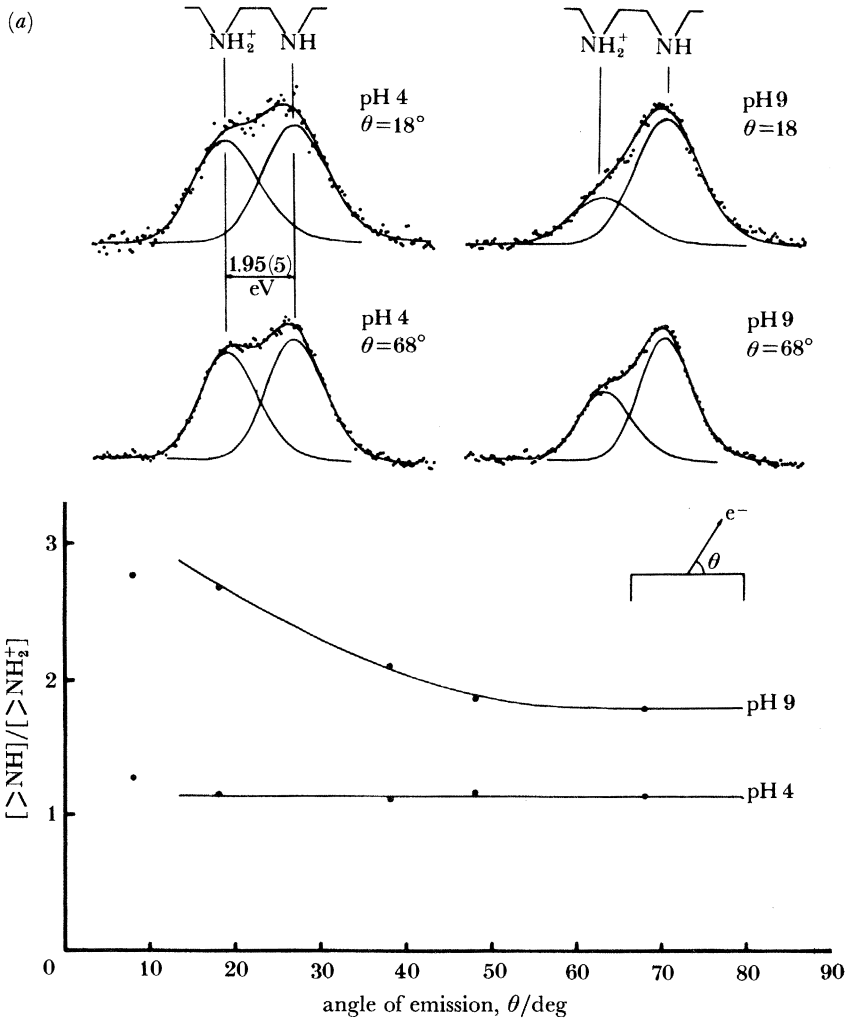

FIGURE 10. Angular dependence (*a*) of the surface-layer lines of the amine–protonated-amine supporting the surface composition shown in the figure (*b*).

different densities of sulphate groups would adsorb different amounts of PEI. So it would be possible to make polymer surfaces with different densities of amine groups not only by adsorption at different pH but also by varying the sulphate group density.

6. Solid–solid interface and the Schottky barrier

Recently a new and much faster alternative to the conventional all-semiconductor npn transistor has been proposed. This substitutes a very thin layer of metal for the base of a standard transistor, thereby dramatically reducing the transit time for electrons from collector to emitter. For such an optimized SMS transistor the theoretical cut-off frequency could be as high as 30 GHz instead of 4 GHz for a GaAs transistor. This SMS transistor consists of a thin layer of cobalt disilicide sandwiched between two thicker layers of silicon, serving as emitter and collector enclosing the $CoSi_2$ base.

Another possible choice is to use a platinum silicide. Previously the metal–GaAs interface has been studied by electron spectroscopy (Waldrop *et al.* 1982; Bauer 1983; Margaritondo 1983; Purtell *et al.* 1983) with the localized core levels used to trace the band bending of the valence band at the interface. For a silicon–silicide interface, however, the problem presented is more difficult because the metal phase itself, which is the platinum silicide, contains silicon that has to be distinguished from the semiconductor silicon. An improved e.s.c.a. (electron spectroscopy for chemical analysis) resolution is then necessary. In a recent investigation (Gelius *et al.* 1984) this problem was studied at a resolution of the diffraction-monochromatized Al Kα line (1487 eV) of *ca.* 0.23 eV. It was then possible to resolve the semiconductor $Si(2p_{\frac{3}{2}})$ core line from the silicide Si(2p) lines of the silicon–platinum-silicide sample. In this way a direct

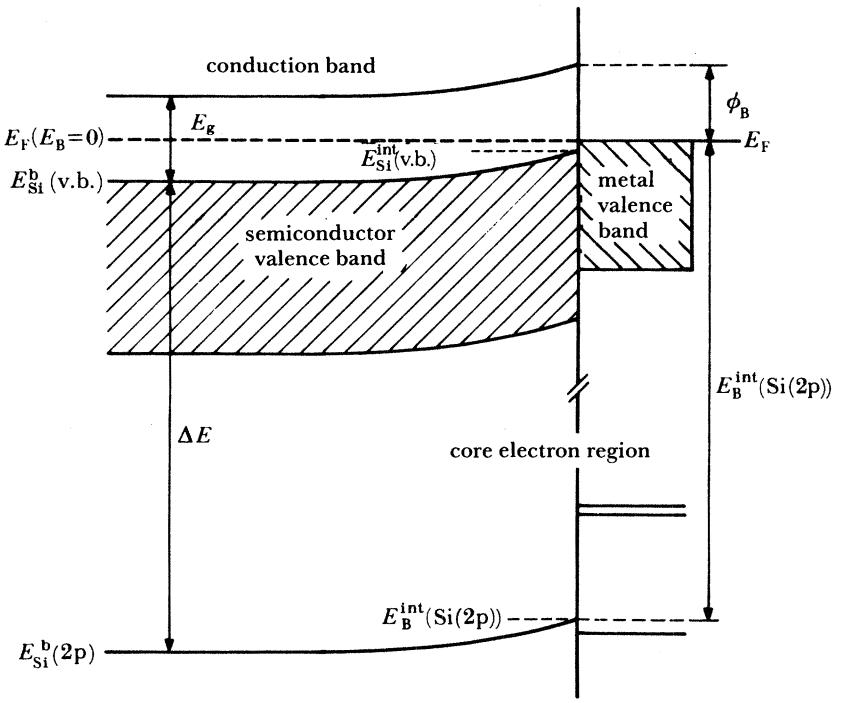

Figure 11. Principle of the e.s.c.a. measurement of a Schottky barrier ϕ_B. The abbreviation v.b. is for valence band; subscripts F, b and g are for Fermi, bulk and gap, respectively; superscript int is for interface.

determination of the Schottky barrier could be made. At this resolution the electron spectrum revealed that the silicide consisted of two chemically different forms, namely PtSi and $PtSi_2$. The e.s.c.a. spectra also showed that on top of the silicide there was a layer of mixed silicon oxides. It was also found that this oxidation took place more easily than for clean Si surfaces, indicating that the presence of metal atoms in the underlying silicide layer has a catalytic promoting influence on the oxidation of silicon.

The e.s.c.a. shifts can to a first approximation be interpreted as corresponding to the potential shift connected with the rearrangement of the valence electron density. In this way one can by means of e.s.c.a. trace the potential distribution that causes the Schottky barrier for a particular metal–semiconductor interface and one can actually measure its value, which in this case was found to be 0.82 ± 0.05 eV. This fits neatly to what has been found by others for PtSi–Si junctions with conventional methods.

The preliminary results on a series formed on the basis of an interface of silicon with a 4–40 Å thickness of platinum silicide seems to indicate that the potential barrier that forms the Schottky barrier might be formed in two steps. The largest step seems to occur between the interfacial silicon atoms and the silicon bulk atoms of the crystal. These findings still require further investigations to enable general conclusions for silicides to be drawn.

The principle of the measurement of the Schottky barrier is illustrated by figure 11. The barrier height ϕ_B is obtained by subtracting the distance between the Fermi level and the silicon valence band from the band gap. From the figure,

$$\phi_B = E_g - E_B^{int}(\mathrm{Si(2p)}) - \Delta E.$$

From an experimental point of view it is necessary that the silicide film is thin enough that the Si bulk line is still observed and that the energy resolution at the required fairly high photon energies (in this case 1487 eV) is high enough to resolve the Si bulk line from the other Si(2p) lines and to allow the observation of the sharp Fermi edge.

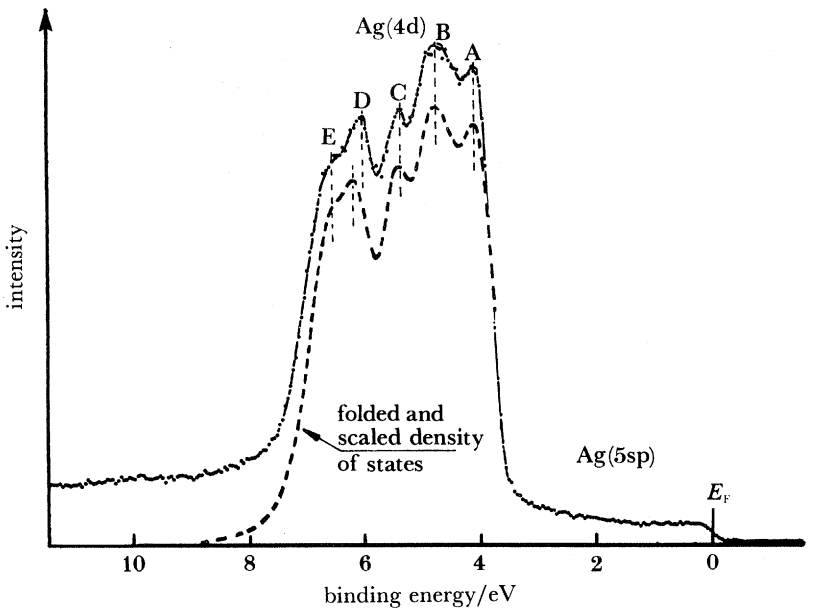

FIGURE 12. The silver conduction-electron band spectrum for $h\nu = 1486$ eV.

7. Conduction bands

The 'state of the art' concerning conduction-band electron spectra is illustrated in figures 12 and 13, which show the Ag and Au bands recorded with our most recent e.s.c.a. instrument (Gelius *et al.* 1984), which was used in several of the studies reported in this review. The resolved structures of the 4d and 5d bands, respectively, correspond in these cases perfectly with structures in the folded and scaled density-of-states functions derived from r.a.p.w. (relativistic augmented plane wave) band-structure calculations indicated in the figures as broken lines (Christensen 1972; Barrie & Christensen 1976).

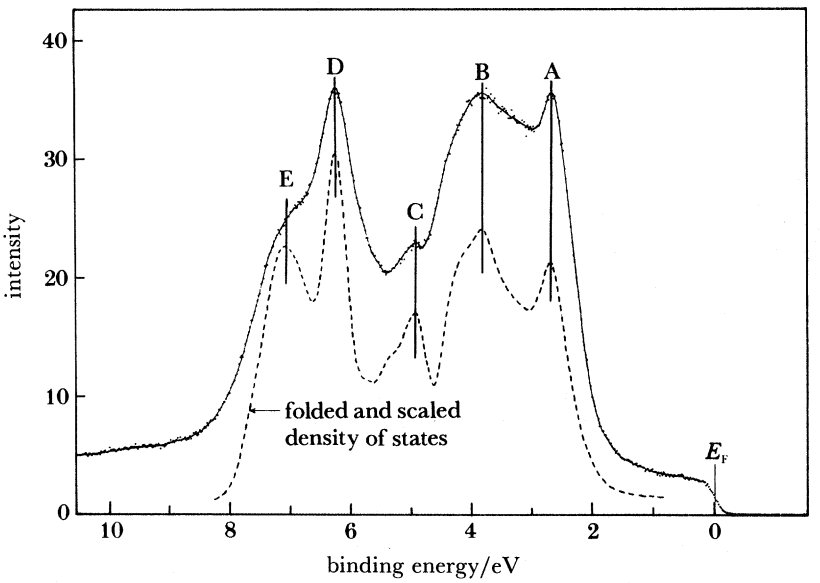

Figure 13. The gold conduction-electron band spectrum for $h\nu = 1486.7$ eV and $\theta = 45°$.

8. Angular distributions and e.s.c.a. diffraction for crystals and adsorbed layers

The angular distribution of electrons emitted from a single-crystal surface covered with adsorbed gas layers gives geometrical information about the positioning of the molecules (see, for example, Mehlhorn 1982). The most discussed example of this is carbon monoxide adsorbed on a Ni(100) surface. One can make use of the dipole selection rule for photoelectron emission to determine whether the CO molecule is standing up perpendicularly or making any other angle to the Ni(100) surface.

Figure 14 shows the principle of such an experiment when linearly polarized u.v. radiation, for example He I at 21.21 eV, is used for the excitation of the photoelectrons. Photoelectrons from an $n\sigma$ orbital can, according to the above selection rule, in general result in $\epsilon\pi$ or $\epsilon\sigma$ final orbitals. If the photons are directed along the axis of the CO molecule only the $\epsilon\pi$ alternative is possible. Turning the plane-polarized electric vector of the photon beam around as in figure 14 and recalling that the $\epsilon\pi$ orbital has a maximum along the electric vector and a nodal plane perpendicular to this direction one should be able to record a zero amplitude in the photoelectron intensity when the electric vector is perpendicular to the emission direction

towards the slit of the electron spectrometer. From such an experiment one can conclude that the CO molecule is actually standing up perpendicularly to the surface in this case.

Experiments of this kind have in general to be combined with extensive calculations concerning continuum wavefunctions and deformations of molecular shapes at surfaces (for example by using cluster calculations). Such calculations are known to be difficult to make (very

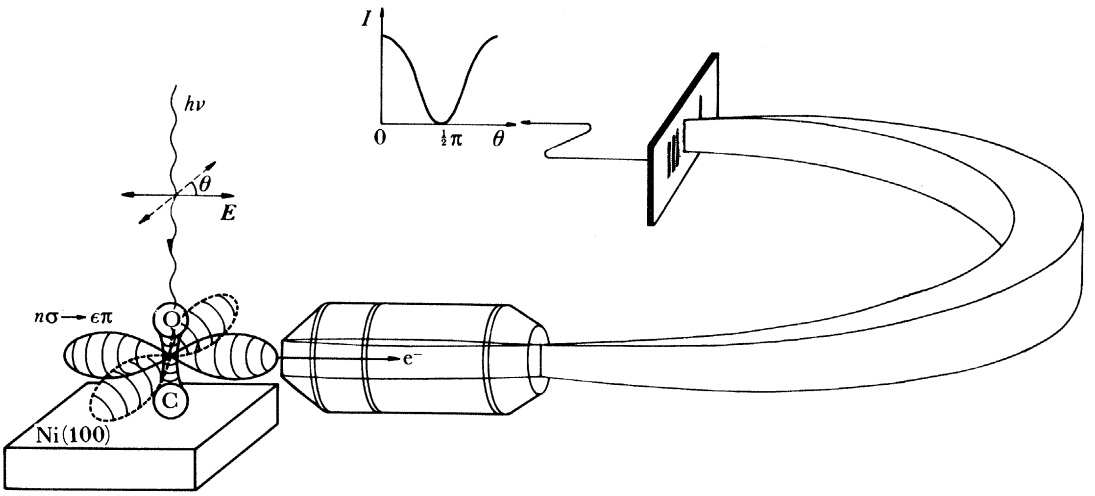

FIGURE 14. Principle for using polarized photons to determine the geometry of adsorbed molecules on a single-crystal surface by the photoelectron angular dependence.

extended basis sets are required) and presently contain great uncertainties. It is likely that new experimental work done for a sufficiently large number of test cases can shed new light on the validity of various such calculations and also eventually lead to semi-empirical approaches in rather more complicated cases than the simple example discussed here.

For the sake of completeness one should be reminded of the angular distributions of photoelectrons from core levels from using (higher energy) photons in the X-ray region, which give rise to e.s.c.a. diffraction patterns. These studies can be made either by recording the angular distributions at fairly small angles (*ca.* 20°) to the surface with a fixed X-ray energy *or* at a fixed angle, for example normal to the surface, and varying the wavelength of the radiation. The latter procedure is especially advantageous with access to the variable synchrotron radiation.

Figure 15 shows an early example of an e.s.c.a. diffraction pattern from a NaCl single-crystal (Siegbahn *et al.* 1970). In this experiment, which has been followed by several others (references are given in Mehlhorn (1982) and recent work is found in, for example, Egelhoff (1984) and Poon & Tong (1984)), it was demonstrated that any core or valence level in any element of a crystal could be studied separately and the corresponding diffraction patterns recorded. This was also demonstrated for the Auger electron diffraction.

Figure 16 shows the principle of this type of diffraction. The primary emitted spherical electron wave is interfering with the secondary scattered electron waves from the neighbouring atoms in the lattice, resulting in an angular dependence of the photoelectron or Auger electron emission intensity. The diffraction peaks along the direction of the lattice points are independent of the wavelength of the (spherical) electron waves and subject to a 'lens' action. Intermediate

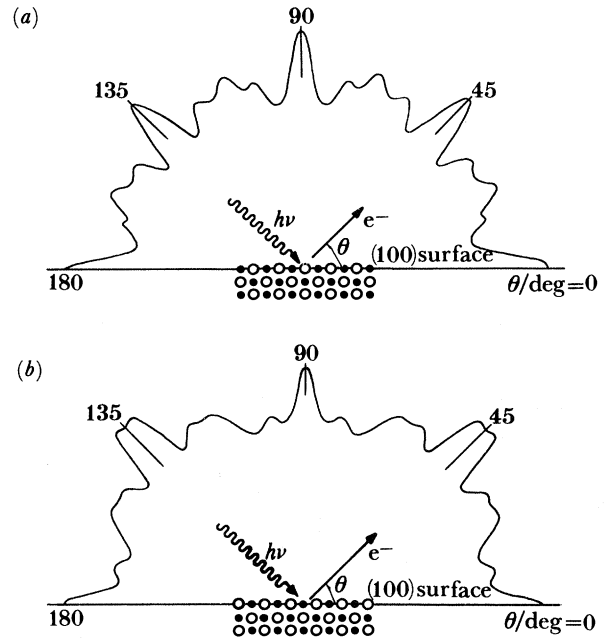

FIGURE 15. E.s.c.a. diffraction for a NaCl single crystal: (*a*) Cl ($2p_{\frac{3}{2}}$), E_{kin} = 1055 eV; (*b*) Na KLL ($^1D_2$), E_{kin} = 990 eV.

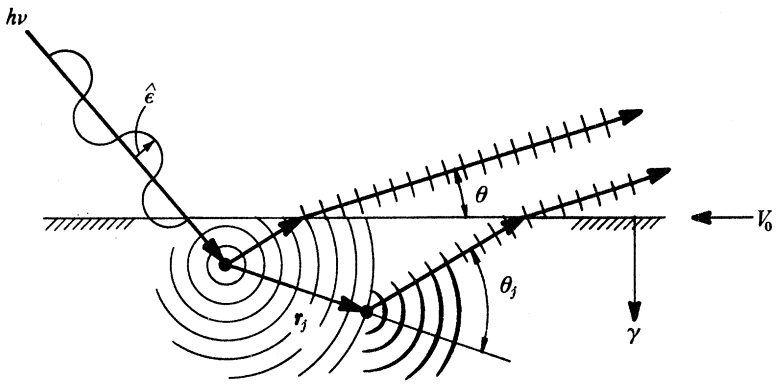

FIGURE 16. Principle of e.s.c.a. diffraction.

directions as indicated in figure 16 are wavelength dependent. It is likely that e.s.c.a. diffraction, in particular for adsorbed molecular surface layers, will be much more extensively studied in the future when the optimum conditions for its practical utilization have been properly realized.

9. ANGULAR DISTRIBUTIONS FOR FREE MOLECULES AND THE β PARAMETER SPECTRUM

The angular distribution of photoelectrons emitted from *free* molecules can be studied either by varying the angle between the direction of the incoming photons and the emitted photoelectrons *or* by using plane-polarized light in a fixed geometry and observing the intensity variations of the photoelectrons as a function of the angle between the electric vector of the

photon beam and the electron emission direction. The latter scheme is much to be preferred from all points of view provided that a photon polarizer of sufficient intensity and beam quality can be realized.

Figure 17 shows a recent design from my laboratory, which follows up the experiences of our previous one, which has been in use for several years. The new design consists of four optical

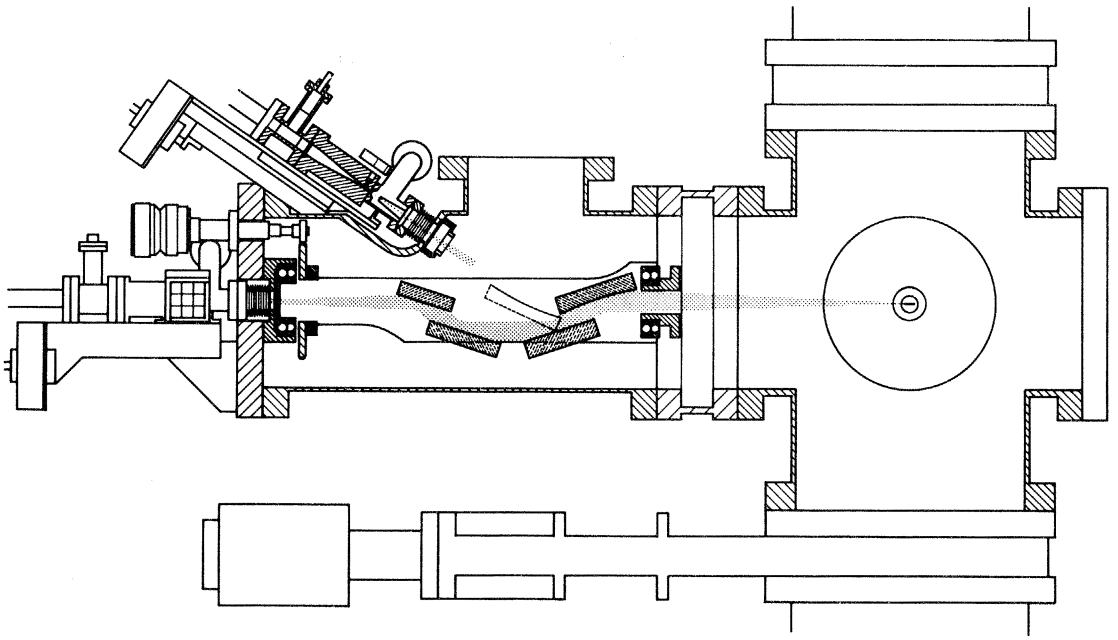

FIGURE 17. Ultraviolet monochromator and polarizer for angular studies of photoelectrons.

elements in the following sequence: one plane mirror, one further plane mirror, one plane grating, one toroidal mirror. This device can be automatically rotated around its axis in a programmed fashion. The focusing in the toroidal mirror compensates for the reflection losses, and also makes it possible to use a large distance between the light souce, polarizer and sample without sacrificing intensity. The last factor is important to minimize the contamination of the reflecting elements, which otherwise makes the polarization decrease with time. By means of the grating, a suitable photon energy can be selected, and with different gases in the light source (H_2, He, Ne, Ar, Kr) the photon energy region 10–51 eV can be covered in small steps.

Some recent examples illustrate the situation for free molecules. For plane-polarized radiation, the intensity distribution of the photoelectrons is given by

$$I(\theta) = I_0(1+\beta/4\,(3P\cos 2\theta+1)),$$

where P is the degree of polarization. The parameter β can then be calculated from the photoelectron intensity parallel and perpendicular to the plane of polarization according to

$$\beta = 4(I_\parallel - I_\perp)/(I_\parallel(3P-1)+I_\perp(3P+1)).$$

The high intensity of the polarized radiation makes it possible and meaningful to calculate the asymmetry parameter β point by point, to generate a 'β parameter spectrum' (β p.s.). Figure 18 is a typical β p.s. showing part of a vibrational sequence of $\tilde{A}\,^2\Pi_u$ in CO_2.

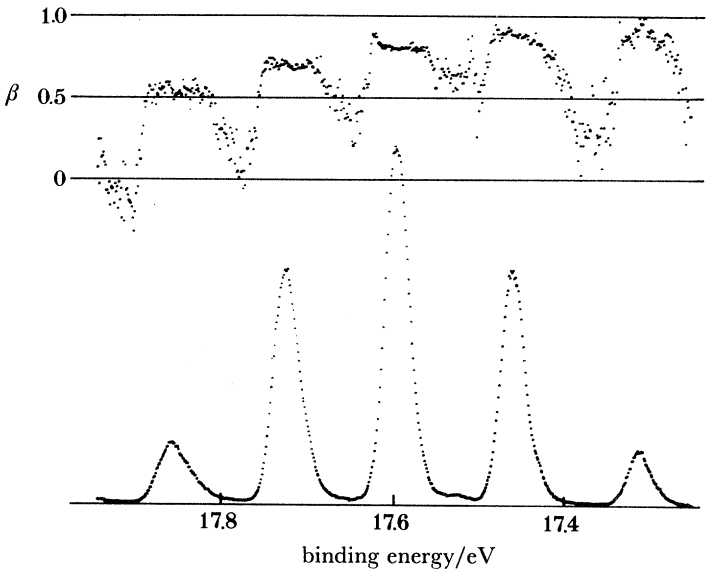

FIGURE 18. A β parameter spectrum (β p.s.) of a vibrational sequence of $\tilde{A}\,^2\Pi_u$ in carbon dioxide for $\theta = 0°$.

Figure 19 shows the photoelectron spectrum of CO and its corresponding β p.s. (Wannberg *et al.* 1985). One first notices the extremely extended vibrational progression in the $\tilde{X}$ state, having 33 vibrational components and covering an energy span of 7 eV. The kinetic energy at $v = 33$ is only 0.25 eV. After a sudden drop in intensity by a factor of 100 from $v = 0$ to $v = 3$, the intensity is fairly constant all the way to $v = 33$. Since the progression overlaps with the other states in CO^+ the energies of the lines can be measured with accuracy and improved values of the anharmonicity parameters can be determined. In the figure the β values at each point of all bands are plotted as a β parameter spectrum. This is done by the computer on line.

For CO_2, the β parameter has been measured for some 40 vibrational states, several of which had not been observed earlier as ordinary photoelectron lines. The β p.s. corresponding to the state $\tilde{X}\,^2\Pi_g$ is shown in figure 20. The prominent β peak at 13.97 eV was found to correspond to the excitation of a single quantum of the antisymmetric stretching mode. In the ordinary spectrum, this line is barely visible as a shoulder on a much more intense peak. This excitation is normally forbidden in photoelectron spectra, but it can attain measurable intensity through interaction with the state $\tilde{A}\,^2\Pi_u$. The large difference in β value between this line and the allowed lines in the $\tilde{X}$-state is characteristic for peaks that get an enhanced intensity through interaction with another state. The β value in such cases tends to come closer to that of the perturbing state than to the state to which it belongs.

The $\tilde{X}\,^2\Pi_g$ state in the CS_2^+ (Norell *et al.* 1984*a*) was investigated by means of a number of photon lines between the H Ly_α (10.20 eV) and He IIα (40.8 eV). Besides the more often used lines from Ne I (16.87 eV), He Iα and Ne II (26.91 eV) a number of lines from discharges in Ar, Kr and Xe were used in the energy region 10.5–13.5 eV. Very rapid oscillations in the β value for the adiabatic transition were observed for kinetic energies of the photoelectron below 4 eV. At the same time the intensity of the vibrational excitation varied. Both these phenomena have to be explained by assuming that the ionization occurs at certain photon energies via

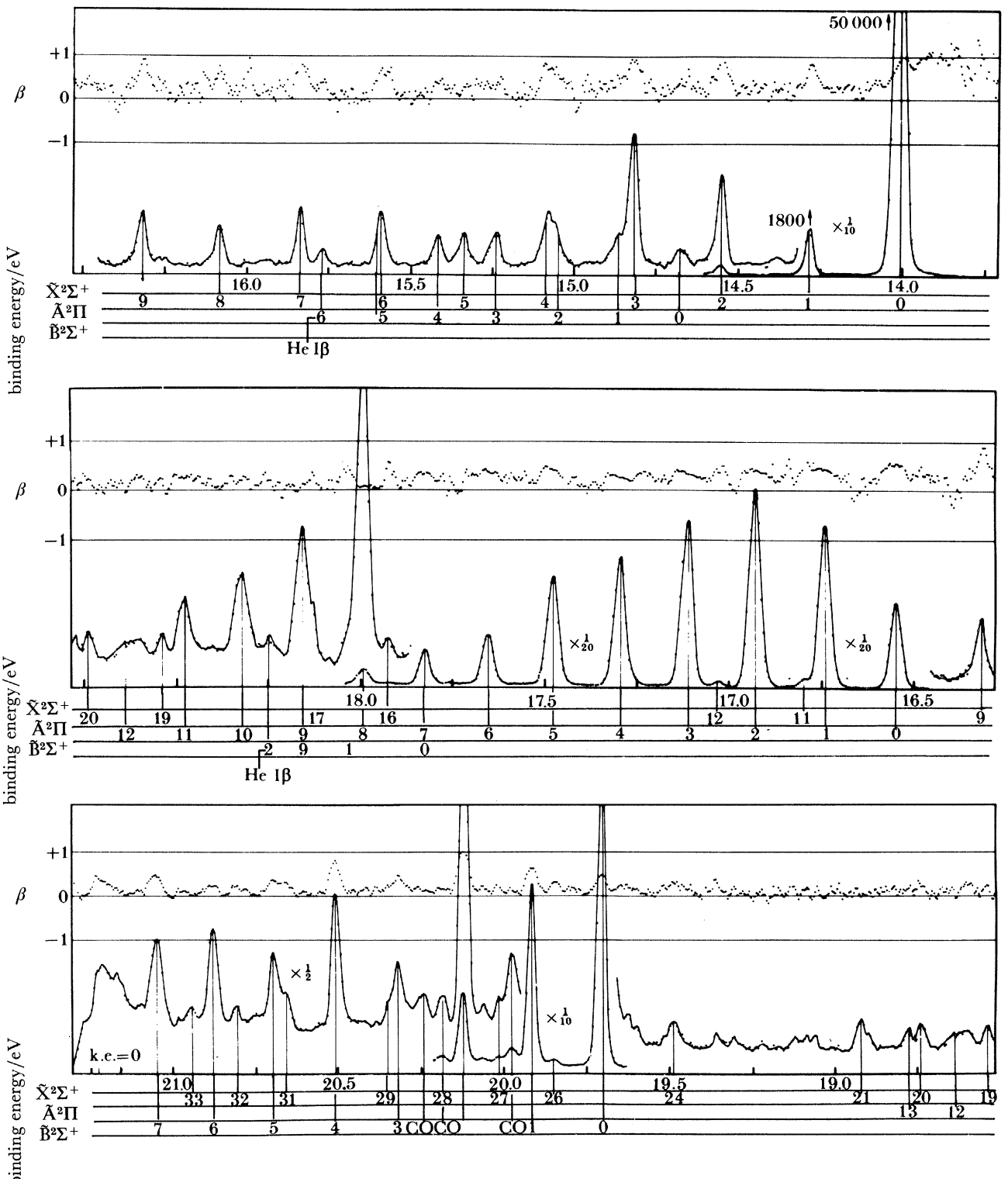

FIGURE 19. The β parameter spectrum of CO. The spectrum contains a vibrational progression in the $\tilde{X}$ state of 33 components.

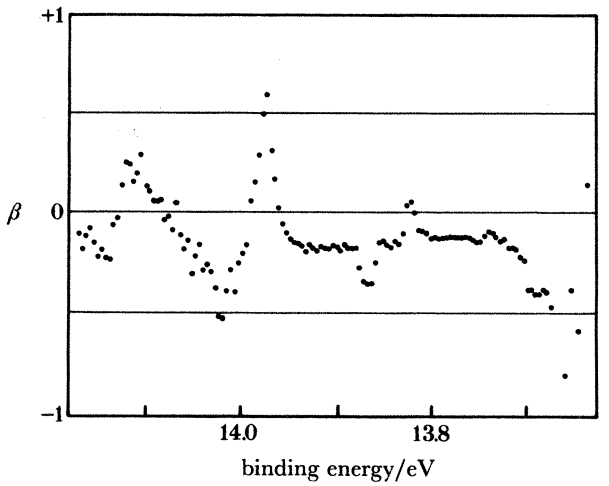

FIGURE 20. A β p.s. corresponding to the state $\tilde{X}\ ^2\Pi_g$ in carbon dioxide around a β peak at 13.97 eV. The enhanced β value is due to an interaction with another state.

autoionizing states. In inelastic scattering events (for example in CS_2) one can distinguish between long-lived intermediate scattering states, which result in a change from non-zero β to zero β and short-lived intermediate scattering states keeping a non-zero β after scattering.

The energy dependence of β close to the threshold for photoionization shows considerable fluctuations. This has been studied in some detail for Ar, Kr and Xe (Wannberg *et al.* 1984*b*). For Kr a deep dip in β for $Kr(4p_{\frac{3}{2}})$ occurred at a photoelectron energy of 581 meV. The β p.s. could be followed down to a photoelectron energy of 15 meV. Such fluctuations can be ascribed to resonances with series of autoionizing states.

When Xe is excited by means of u.v. radiation from a discharge in N_2 one can study the β parameter spectrum close to the ionization threshold, in particular in the region between the thresholds for ionization of the $p_{\frac{3}{2}}$ and $p_{\frac{1}{2}}$ states. There is a sufficiently large number of closely spaced u.v. lines from N_2 in the discharge available for ionization of Xe at all photon energies of interest. As can be seen in figure 21, the photoelectron spectrum taken parallel to and perpendicular to the electric vector of the N_2 photon beam both reflect the complicated structure of the exciting photon spectrum coming from N_2 in the discharge source, 'scanned' by the p level of Xe in the photoelectron spectrometer. However, from the *ratio* of the intensities at each photoelectron energy the β parameter spectrum of Xe can be derived, as shown in the upper part of the figure. This β p.s. contains an interesting sequence of minima, consisting of a converging series of resonances. This can be understood in terms of a series of autoionizing states in Xe, which converges towards the $p_{\frac{1}{2}}$ ionization limit. The figure also shows that the β parameter can be measured down to a few millielectronvolts above the ionization threshold.

In conclusion one can forecast a rapidly expanding area of research related to the angular dependence of photoelectrons as a function of energy both at threshold and at higher energies by means of polarized light.

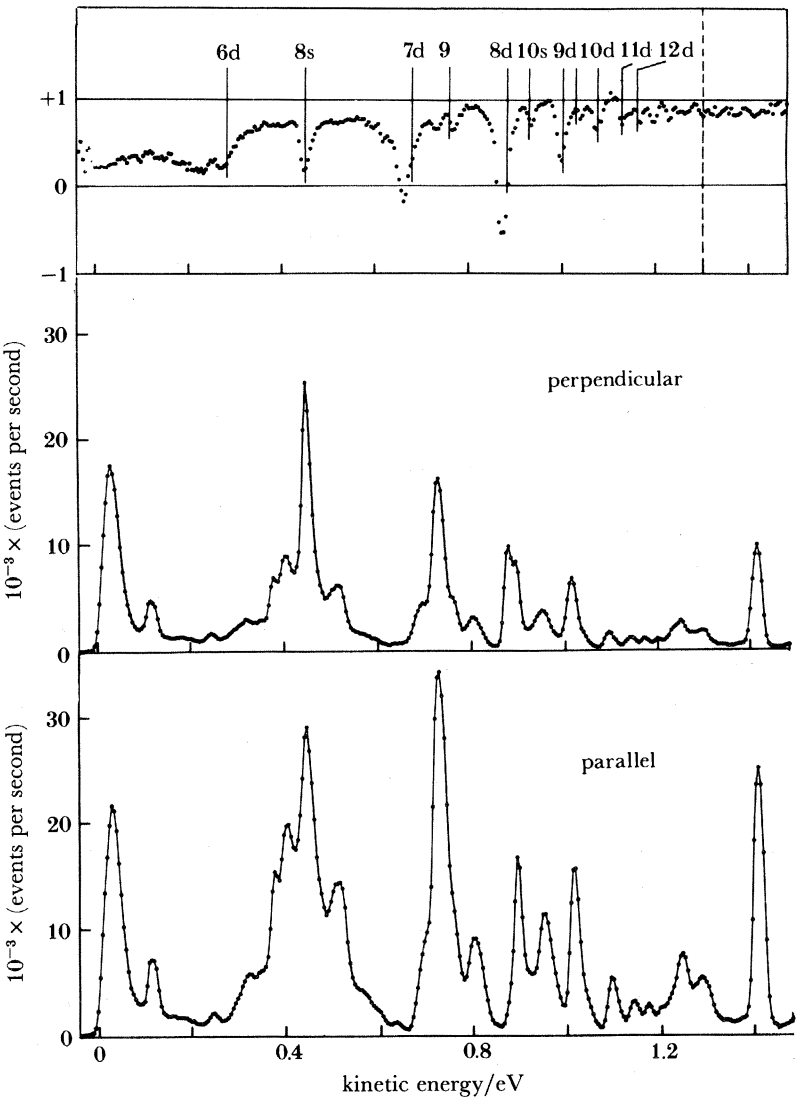

FIGURE 21. The β p.s. of Xe in the region between the threshold for ionization of the $p_{\frac{3}{2}}$ and $p_{\frac{1}{2}}$ states with use of N_2 in the light source.

10. LIQUIDS AND SOLUTIONS

In this review I have so far discussed some fields in electron spectroscopy that concern the solid state, in particular surface properties, and also some examples concerning free molecules in the gaseous state. The third state of aggregation, the liquid state, now remains to be discussed. This is a fairly new field in electron spectroscopy and most of the applications will be more fully explored in the future. Since this field has recently been developed some of its fundamentals might be reviewed here.

One can distinguish between the *liquid–vacuum* interface with challenging problems analogous to the solid–vacuum interface and the *solid–liquid* interface. The latter has so far only been studied in a few cases by means of electron spectroscopy. In principle this could be achieved by a continuously renewed extremely thin liquid film on top of a solid surface and a

correspondingly hard X-radiation to expel photoelectrons with a large enough escape length to penetrate the liquid layer. There is, however, a much better probability for success by the reverse procedure, namely to create a thin solid surface layer on top of a liquid. Again the X-radiation has to be hard enough to produce electrons in the interface that are able to penetrate the thin solid film. This is similar to the problem discussed above dealing with the silicide–silicon interface. By using monochromatic and focused Al Kα radiation the liquid–solid interface has been accessible for recording in a few cases in our laboratory, for example hydrocarbon films on liquids. Further investigations along these lines are in progress.

The liquid–vacuum interface would rather be called liquid–gaseous since most liquids have non-negligible vapour pressures. This is one of the main obstacles in liquid electron spectroscopy. When we started this field we were aware of this problem from our previous studies of gases, where arrangements had to be made for the differential pumping of the gases. Most of the polar liquids that are of interest in chemistry as solvents do have a rather high vapour pressure at ordinary temperatures. In particular, water, but also many other liquids, would not be accessible for liquid electron spectroscopy unless a sufficiently hard radiation is used, if one requires a reasonable signal: background ratio and also decent line shapes in the spectra.

Another demand on the experimental arrangement is that the liquid surface is kept fresh continuously. This can be accomplished by renewing the liquid in front of the electron spectrometer slit all the time. There are several ways to do this by translational or rotational arrangements. Several of these have been tested and used for extended periods of time and they work satisfactorily. There are further schemes now under study which look promising for certain problems, for example the penetration of liquids and solutions through membranes, some of which are of biological interest. Studies of water solutions require some special arrangements.

Already our early recordings of X-ray excited liquid spectra have produced well defined photoelectron and Auger electron lines, which well fulfilled the requirements on line shapes and signal: background ratio (Siegbahn 1985). The liquid spectra looked very similar to those previously obtained for solids not only in the core-electron region but also in the valence region, the latter first demonstrated for formamide.

The valence region is within reach also by means of the He resonance radiation at 21.21 eV (Delahay 1984; Ballard *et al.* 1983). There seem, however, to be serious problems here for liquids with respect to line shapes and signal: background ratio, which greatly reduce the applicability of this approach. Whether this is due to inherent basic problems connected with the small mean free paths for the photoelectrons in the liquid and in the surrounding vapour phase or due to other shortcomings remains to be further studied.

Electron spectra excited by monochromatic and focused Al Kα radiation exhibit well defined line shapes and good signal: background ratio and this technique is very well suited for liquids. The following text concerns the results of these investigations. Core-electron spectra contain information about ionic behaviour and relaxation phenomena in liquids that can be related to the chemistry of solutions, which will be discussed here.

The fields of interest are:

(1) ions in solution (electronic structure and dynamics, solvation and reaction energies, complex formation and colloids);

(2) intermolecular forces (valence-level effects; core-level effects);

(3) liquid–vacuum interface (surface-active species);

(4) molten substances.

As for metals it is convenient to be able to correlate the positions of the measured liquid lines

to a reference level, preferably the vacuum level, to arrive at a consistent picture that enables direct comparison to be made between the gas-phase and the liquid-phase binding energies. This is achieved in the following way. The liquid sample plus the metal backing in contact with the liquid during the movement of the sample (for example a translational wire or a rotational trundle) form together an electrochemical half cell. One can express the electromotive force of this half cell in terms of thermochemical entities (heat of evaporation and solvation) related to the creation of an ion and its transfer from the metal electrode into the bulk of the solution. The e.m.f. of this half cell can be experimentally determined by connecting it to a reference electrode. The liquid surface and the reference electrode thus form a condensor pair whose potential difference (Volta potential) can be determined by vibrating the reference electrode (vibrating condensor method). The energy-level scheme in the liquid e.s.c.a. arrangement is illustrated in figure 22. From the figure one can deduce the relation between the liquid- and gaseous-phase e.s.c.a. spectra. For the liquid lines, for example the core lines of a metal ion or the C(1s) line of an organic solvent:

$$E_{\mathrm{kin}}(\mathrm{liq}) = h\nu - E_{\mathrm{B}}^{\mathrm{V}}(\mathrm{liq}) + \phi_{\mathrm{Volta}}.$$

$E_{\mathrm{B}}^{\mathrm{V}}$ is the binding energy referred to the vacuum level. The gaseous-phase photoelectrons are created within the Volta potential field and they will thus not experience its full effect but only

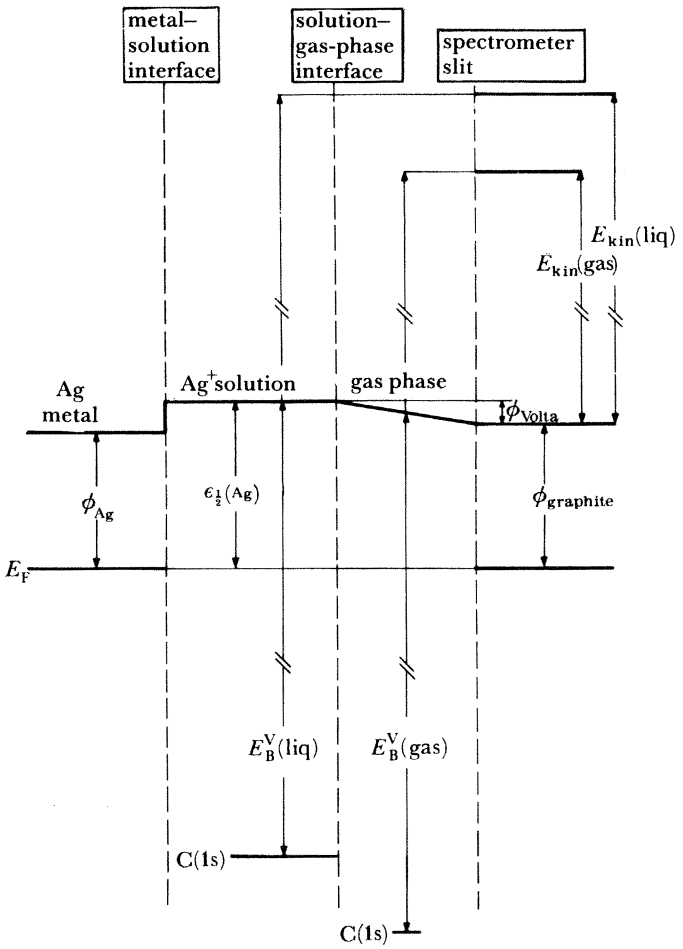

FIGURE 22. Relation between liquid and gas e.s.c.a.

about half, on average. Let us account for this through the factor k, which is a directly measurable quantity in the arrangement used, described below. Then for the gaseous phase:

$$E_{\mathrm{kin}}(\mathrm{gas}) = h\nu - E_{\mathrm{B}}^{\mathrm{V}}(\mathrm{gas}) + k\phi_{\mathrm{Volta}}.$$

The two equations give together:

$$\mathrm{E}_{\mathrm{kin}}(\mathrm{liq}) - E_{\mathrm{kin}}(\mathrm{gas}) = E_{\mathrm{B}}^{\mathrm{V}}(\mathrm{gas}) - E_{\mathrm{B}}^{\mathrm{V}}(\mathrm{liq}) + k\phi_{\mathrm{Volta}}.$$

If the sample backing is made of silver and the spectrometer and the slit is painted with aquadag the Volta potential is

$$\phi_{\mathrm{Volta}} = \epsilon_{\frac{1}{2}}(\mathrm{Ag}) - \phi_{\mathrm{graphite}},$$

where $\epsilon_{\frac{1}{2}}$ is the e.m.f. of the half cell. These are the expressions that refer the measured liquid lines to the vacuum level by using a gas line as a reference line.

Figure 23 shows the C(1s) spectrum from ethylene glycol by using a simultaneous inlet of CO_2 gas as reference. Three different half cells were studied: $(Zn|Zn^{2+})$, $(Cu|Cu^{2+})$ and $(Ag|Ag^{+})$. According to the equations given the liquid line should shift in kinetic energy from one case to another by the difference in cell e.m.f., i.e. by the cell e.m.f. consisting of the two half cells. The gas lines, on the other hand, should shift by only about half this quantity (dependent on the value of k). This means that the gas–liquid shift will increase as the half cell e.m.f. increases. This is also what happens in the experiment according to figure 23.

Figure 24 summarizes the experiments and verifies the validity of the above formulae. The

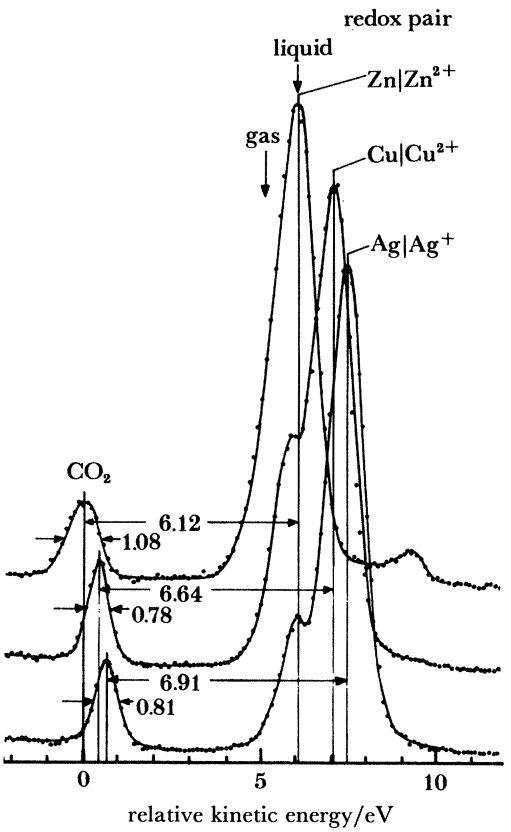

FIGURE 23. C(1s) core lines in ethylene glycol with CO_2 as reference gas. Three different half cells.

straight line connecting the points is not a fit, but is experimentally determined by removing the liquid sample and letting in Ne gas instead. The position of the Ne(1s) line was then measured as a function of potential applied to the liquid backing. In this way the constant k was determined to be 0.45. The calibration of the liquid e.s.c.a. arrangement can be effected with good accuracy and the core and valence liquid lines can be measured with the same accuracy and referred to the vacuum level. Calibrations are made for the solvent lines of certain selected cases. For routine work the energies of unknown lines are calibrated against the solvent lines, previously measured. It should be emphasized again that the basic condition for the fruitful use of e.s.c.a. for liquids is that electron lines of good quality are obtained. It is gratifying to state that this condition is well fulfilled, as further exemplified by figures 27, 28, 29 and 31 (which appear later).

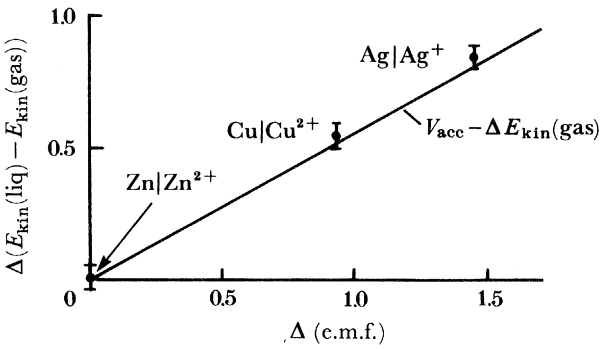

FIGURE 24. Verification of formula according to figure 22.

Core-electron spectroscopy gives information about the electron charges around atoms, since the potential is affected at the formation of different chemical compounds of a given element. The change of charge at the photoelectron emission process of one unit for photoelectron lines and two units for the Auger electron process will be followed by a relaxation of the atomic electrons when the hole state is being formed. This is the origin of the relaxation energy. The difference in relaxation energies between two compounds can be determined by measuring both the photoelectron energy shifts and the Auger electron energy shifts. The relation between the three quantities is

$$\Delta E_{relax} = \tfrac{1}{2}(\Delta E_B + \Delta E_{Aug}).$$

The relaxation energy is, for liquids, directly related to the solvation energy of a certain ion in a solution. The solvation energy is defined as the energy released when an ion is transferred from vacuum into the bulk of the solvent.

The solvation energy can be divided into a number of hypothetical steps, as illustrated in figure 25. First, a cavity is created in the solvent large enough to precisely fit the ion. The energy for this step (E_{cav}) is practically equal to the solvation energy of a noble gas (E^{ng}_{solv})). In the next step, the molecular dipoles are ordered to form a solvation shell for the ion (E_{ord}). The energy loss associated with introducing this strain in the liquid ($E_{str} = E_{cav} + E_{ord}$) is gained back when the ion is fitted into the cavity. This energy gain may be divided into two contributions, one associated with the interaction of the ion with the permanent dipole moments of the molecules ($E_{ion-dip}$) and another associated with the induced electronic polarization of the molecules by the ionic electric field (E_{el-pol}).

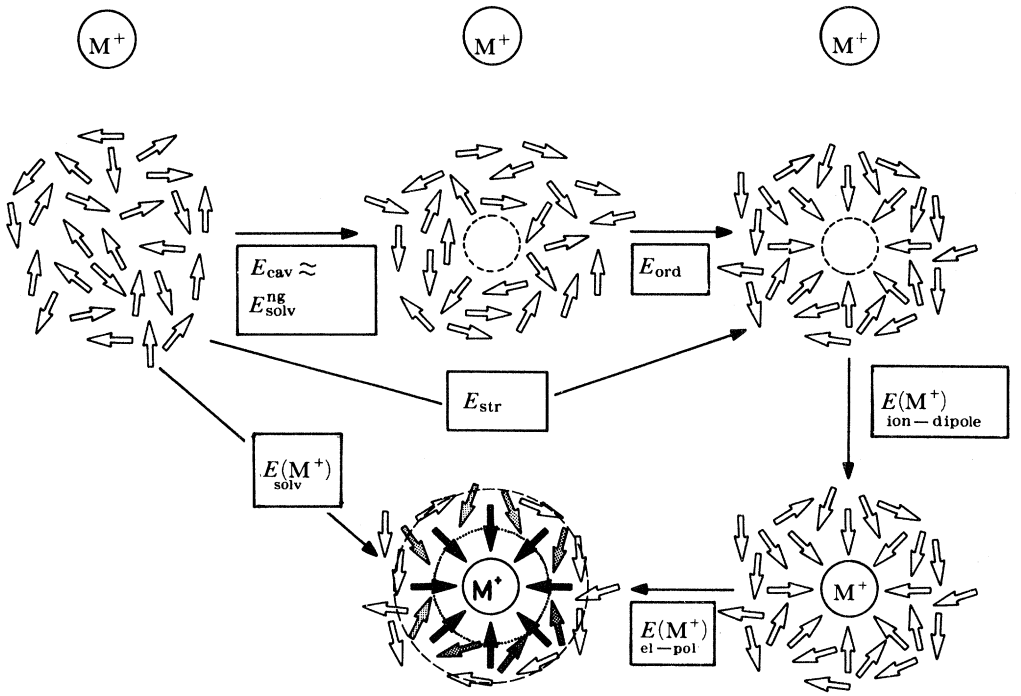

FIGURE 25. Solvation of ions in hypothetical steps.

Figure 26 illustrates the application of core electron spectroscopy to the investigation of metal complexes in solution. The figure shows how measured core-electron binding-energy shifts and Auger electron-energy shifts between the gaseous and the liquid phase can be related to solvation energies via a Born–Haber cycle. Since the solvation energy is essentially the energy associated with the reaction of the solvent against a dissolved ion it corresponds to the previously discussed relaxation energy. As indicated the molecules of a solvent can react in two ways

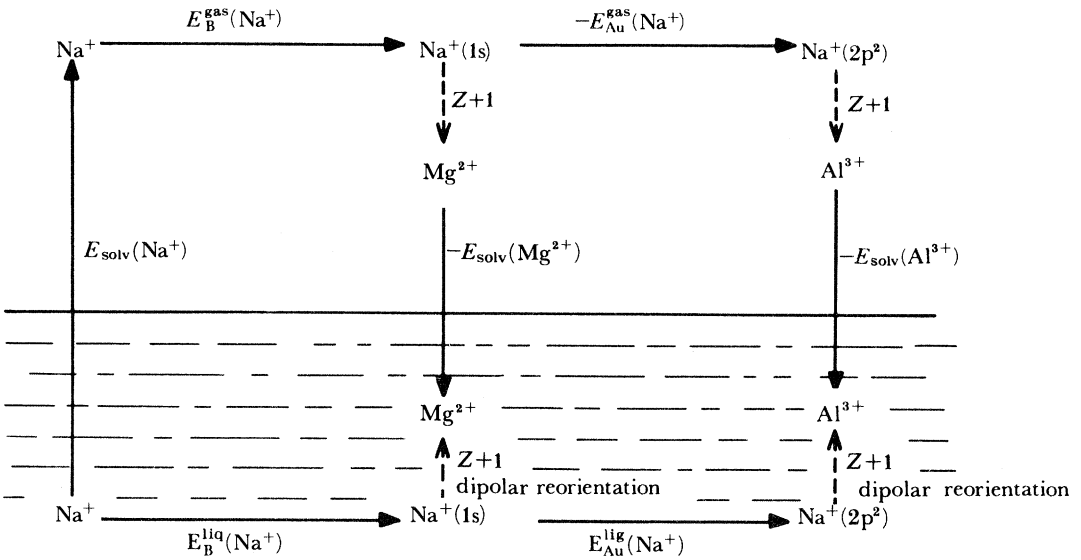

FIGURE 26. Born–Haber cycle for core spectroscopy of metal complexes in solution.

against a dissolved ion: (1) by a fast electronic polarization and (2) by a slower reorientation of their electric dipoles.

The relaxation energy that is being measured in the fast e.s.c.a. process is that associated with the electronic polarization, which takes place within the order of 10^{-15} s, whereas the dipolar reorientation takes a much longer time. Therefore, the two contributions to the chemically measurable *solvation energy can be separated into independent parts* in the cases when the total solvation energy is measured by thermochemical means.

Returning to the Born–Haber cycle, one may recall that ions in an electrolyte mostly have closed-shell rare-gas electronic configurations. Core-electron spectroscopy is therefore particularly advantageous since it allows comparison to be made between isovalence-electronic species such as Na^+, Mg^{2+}, Al^{3+}, etc., for which accurate thermodynamic data are available. In the particular case illustrated here, ls ionization of Na^+, accurate figures can be obtained for the reorientation energies associated with the change from a Na^+ to Mg^{2+} or a Al^{3+} ion.

Figure 27 shows a core- and Auger-electron spectrum of a solution of Na^+I^- (5 M) in glycol. The shifts of the Na^+ lines with respect to the gas phase (solvation shifts) were obtained from photoelectron spectroscopical atomic gas phase data combined with calculated atom–ion shifts (using simple s.c.f. routines). Figure 28 shows the liquid e.s.c.a. spectrum of $SrBr_2$ (1 M). The Br^--gas value was obtained from a molecular photoelectron spectroscopical value coupled with a calculated molecule–atom shift and an atom–ion shift. Figure 29 is the e.s.c.a. spectrum of $HgCl_2$ (0.2 M) in C_2H_5OH. Observe the e.s.c.a. chemical shift between the two carbon atoms in the ethyl group.

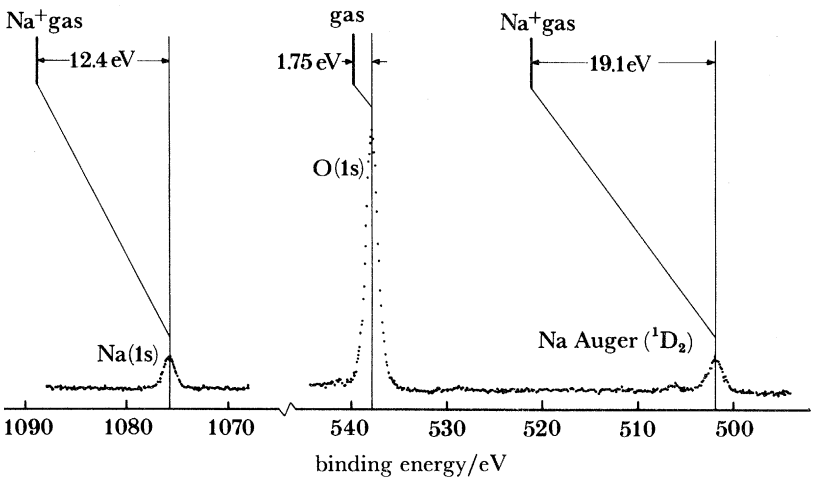

FIGURE 27. Core and Auger electron spectrum of a solution of Na^+I^- (5 M) in glycol.

The Auger energy shifts play an important role in that the different contributions defined in figure 26, associated with the solvation of an ion such as Na^+, can be obtained via a combination with the corresponding binding energy shift. The electronic polarization contribution is obtained from

$$E_{\text{el-pol}}(Na^+) = \tfrac{1}{2}(\Delta E_B(Na^+) + \Delta E_{Aug}(Na^+)).$$

This follows from the equation for the relaxation energy given above. Further, the interaction energy of the ion with the molecular dipoles is given by (Siegbahn *et al.* 1983)

$$E_{\text{el-pol}}(Na^+) = -\tfrac{1}{2}(5(\Delta E_B(Na^+) + 3\Delta E_{Aug}(Na^+)).$$

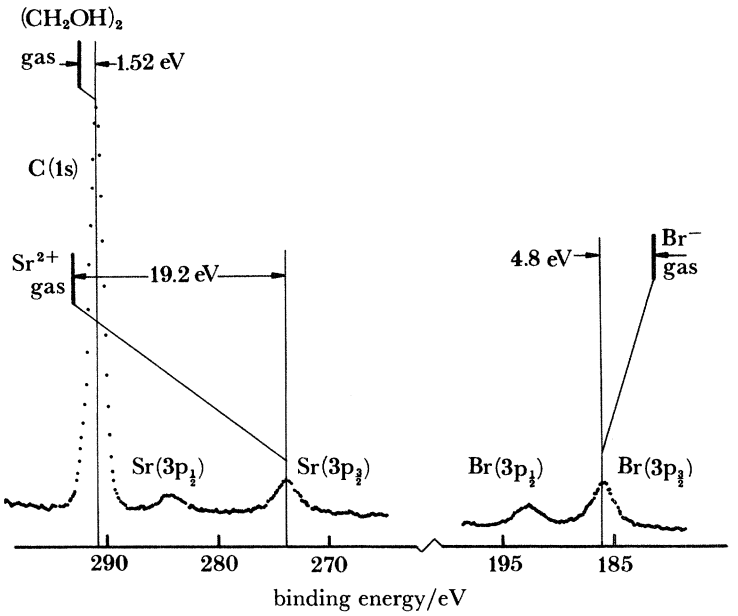

FIGURE 28. Liquid e.s.c.a. spectrum of $SrBr_2$ (1 M).

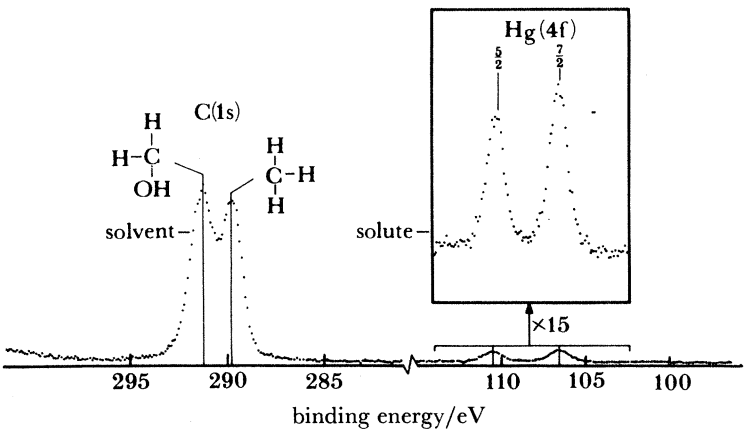

FIGURE 29. E.s.c.a. spectrum of $HgCl_2$(0.2 M) in C_2H_5OH at −85 °C.

Using these two values and the solvation energy for the ion (measured thermochemically) one can deduce the strain created in the solvent when the ion is dissolved in it:

$$E_{\mathrm{str}}(\mathrm{Na}^+) = E_{\mathrm{solv}}(\mathrm{Na}^+) - E_{\mathrm{el\text{-}pol}}(\mathrm{Na}^+) - E_{\mathrm{ion\text{-}dip}}(\mathrm{Na}^+).$$

Recent systematic studies by e.s.c.a. show that at low-valence states of the ion the two contributions to the solvation energy are about equal, whereas at higher valence states the electronic polarization contribution is becoming the more important part. Figure 30 shows the result of such a study for Na^+.

The experimental e.s.c.a. studies of liquids can be complemented by model calculations of the solvation shifts of core levels. It is reasonable to assume that solvation binding energies and Auger energy shifts of ion energy levels are to be described within a model that combines the

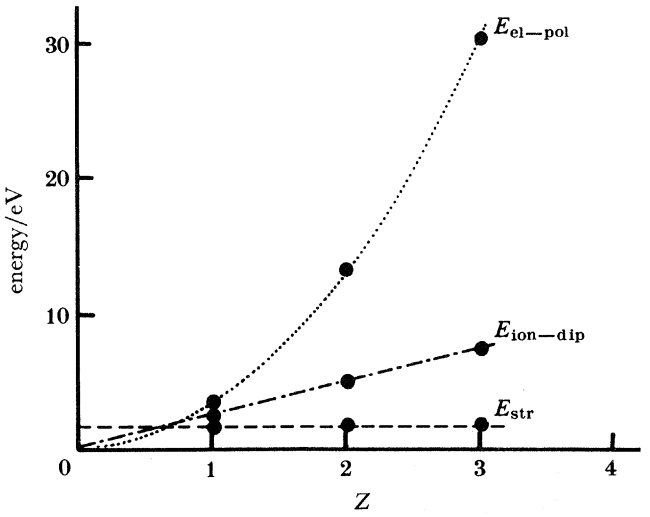

FIGURE 30. The different contributions to the solvation energy as a function of valence state.

long-range continuum-like behaviour of the solvent with a short-range molecular interaction between the ion and first solvation shell of molecules.

In particular, to study the latter part and also assess the importance of the long-range interaction, *ab initio* calculations have been made on Na^+ solvated clusters surrounded by an increasing number of molecules (Arbman *et al.* 1985). For a proper comparison with experimental data in solution it is desirable to perform calculations up to and including a fully solvated cluster with six solvent molecules. This is practically possible only for water ligands and carefully chosen basis sets. Calculations for other solvent molecules (such as methanol) must then be made for a more limited number of molecules and results extrapolated to full clusters. The main results of the calculations are given.

(1) The experimental cluster solvation energies for Na^+ (H_2O) are reproduced with a high accuracy by using a basis set of moderate size including polarization functions of p-type on ligand molecules.

(2) The calculated binding and Auger energy solvation shifts for the cluster are smaller by at least 20% compared with experimental values obtained in solution. The discrepancy is moreover substantially larger for the Auger shift. This reflects the importance of long-range electronic polarization in the description of the solvent environment of small cations in solution. This electronic polarization becomes increasingly important for higher charge states of the ion. A cluster model is generally insufficient to reach the values obtained in ionic solutions by electron spectroscopial means.

(3) Replacing H_2O as ligand with CH_3OH results in an overall increase of the binding energy and Auger shifts of *ca.* 20%. This may be rationalized as an effect of the increasing number of polarizable valence electrons in the cluster. The methanol cluster (with the same number of molecules at the water cluster) can be considered as a structure with more than one solvation shell.

The field of liquid e.s.c.a. is at present in an interesting stage of development. One of the next steps to be taken is the study of *water* solutions, in which case the high vapour pressure is an experimental obstacle. Figure 31 is the first example of this, which shows the liquid and

the gas O(ls) lines from water in a saturated LiCl solution (Lundholm *et al.* 1985). The vapour phase line has been removed in the upper spectrum by applying a small potential on the liquid-water backing. This affects the vapour line in such a way that it broadens and actually disappears into the background whereas the liquid-water line is only shifted by an amount corresponding to the applied potential, but with an unaffected line profile. This simple trick has turned out to be a general method to produce clean liquid spectra without the interference of the simultaneously occurring vapour lines.

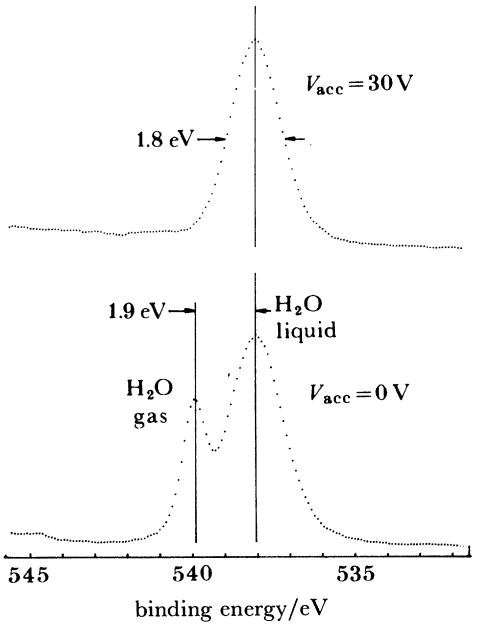

FIGURE 31. Spectrum of liquid water at 254 K. The O (ls) water–gas line is removed by applying a potential on the backing of the liquid sample. The remaining O(ls) is from liquid water alone.

Other possible applications include biological systems and the transport of electrolytes through membranes. Again, such experiments require additional techniques to be developed in electron spectroscopy. Chemical surface reactions in the gas–liquid interface are other typical problems suitable for e.s.c.a. studies.

11. RECENT DEVELOPMENTS

I end this review by briefly mentioning a forthcoming field in its infancy, namely the investigation of excited or fragmented molecular systems by means of electron spectroscopy. The molecules can, before being ionized, be subject to various treatments: pyrolysis, electron swarm treatment, microwave heating or laser irradiation. One may describe this development as proceeding from 'static' electron spectroscopy dealing with the molecules in their ground states to 'dynamic' electron spectroscopy when they are excited or fragmented to form free radicals.

A recent experimental arrangement to make such and several other experiments in electron spectroscopy is shown in figure 32. (A further scheme using time-of-flight techniques in a magnetic bottle is described by Norell *et al.* 1984*b*.) The main scheme under development is

a spherical analyser equipped with two independent ports, one for u.v. or electron-beam excitation (electron energy loss spectroscopy) combined with laser irradiation of the molecules (or surfaces), the other X-ray excitation by using diffraction monochromatized and focused X-rays of increasing order at Al $K\alpha = 1486.65$, Ag $L\alpha = 2984.41$, Ti $K\alpha = 4511.0$ and Cr $K\beta = 5946.91$ eV. The latter port is suitable also for liquid studies, for example water solutions. Any of the available ports can be used in connection with other external radiation sources, for example laser or synchrotron radiation. The instrument is built in a modular system to facilitate various changes in the experiments or to add other equipment, for example Auger electron guns, different types of X-ray or u.v. sources and u.h.v. sample-preparation chambers. It is equipped with a u.v. monochromator with variable photon energies between 10–51 eV and also with the four-component polarizer for the same energy span mentioned above (figure 17). The polarizer can be rotated around its axis, which connects the u.v. light source and the sample slit. A new v.u.v. source has been developed for this instrument. It is based on a microwave (X-band) discharge, where the electron density and energy are increased by means of an

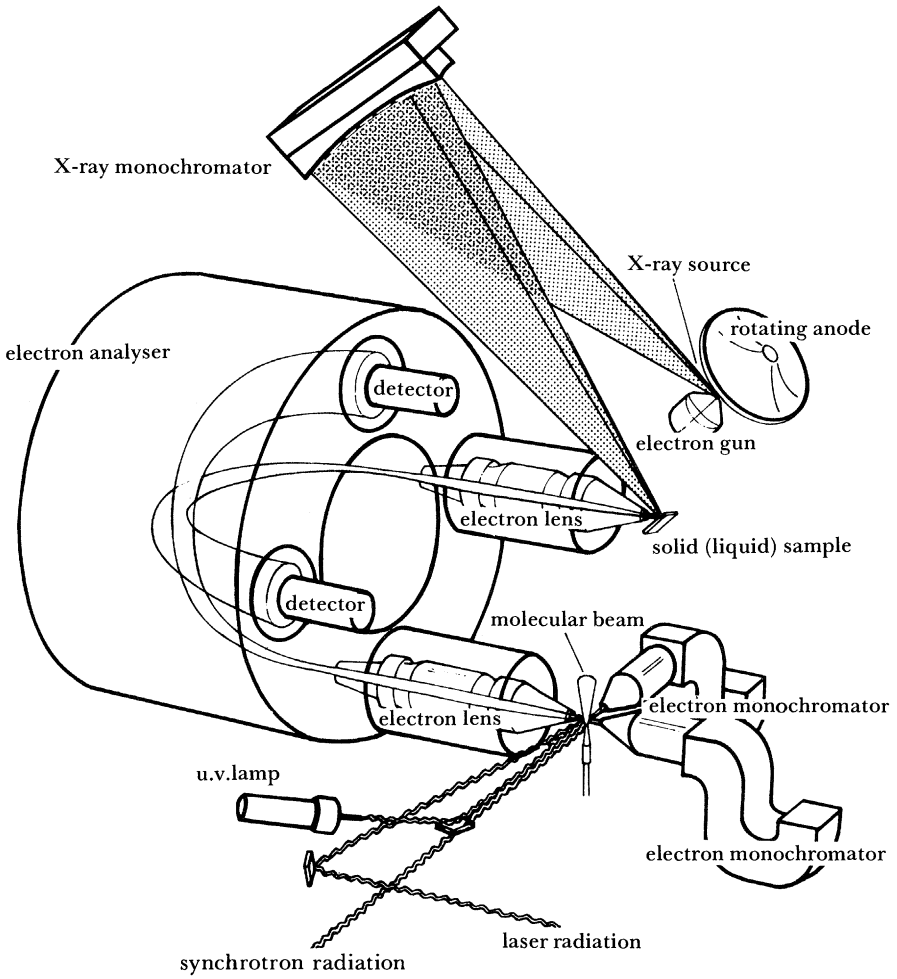

FIGURE 32. New instrument for combined e.s.c.a. with laser radiation. Molecules (or surfaces) are affected by a laser beam and ionized in front of the electron spectrometer slit. The instrument is provided with different sources of excitation in a modular fashion, monochromatized X-radiation, u.v. radiation and monochromatized electrons.

external magnetic field across the cavity, tuned to fulfil the electron cyclotron resonance condition at the microwave frequency. This makes it possible to work at much lower gas pressure in the discharge than in other light sources, thus effectively reducing the self-absorption broadening of the resonance radiation lines (Baltzer 1985, unpublished work). To reach increased resolution for free molecules the Doppler broadening due to thermal motion and also the rotational broadening has to be reduced. The apparatus is therefore constructed for efficient differential pumping to enable the use of supersonic molecular jet beams. A main feature of the installation is the combination of laser irradiation of the sample and the ionizing radiation, which will provide the prerequisites for the above-defined dynamic electron spectroscopy. A further approach is the ionization by two-photon laser excitation with resonances at the intermediate-state photon absorption, which provides information on these states.

References

Arbman, M., Siegbahn, H., Pettersson, L. & Siegbahn, P. 1985 *Molec. Phys.* **57**, 1149.

Ballard, R. E., Jones, J., Sutherland, E. & Chun, B. L. 1983 *Chem. Phys. Lett.* **87**, 419.

Barrie, A. & Christensen, N. E. 1976 *Phys. Rev.* **B 14**, 2442.

Bauer, R. S. 1983 *Phys. Lett.* **43**, 663.

Christensen, N. E. 1972 *Physics Status Solidi* **B 54**, 551.

Delahay, P. 1984 In *Electron spectroscopy, theory, techniques and applications* (ed. C. R. Brundle & A. D. Baker), vol. 5, pp. 123–196. London: Academic Press.

Egelhoff, W. F. Jr 1984 *Phys. Rev.* **B 30**, 1052.

Gelius, U., Asplund, L., Basilier, E., Hedman, S., Helenelund, K. & Siegbahn, K. 1983 *Nucl. Instrum. Meth.* **1**, 85.

Gelius, U., Helenelund, K., Asplund, L., Hedman, S., Tove, P. A., Magnusson, K. & Jain, I. P. 1984 *Uppsala Univ. Inst. Phys. Rep.* no. UUIP-1101, *Proc. of ICTF-6 Stockholm, 1984.*

Gelius, U. & Siegbahn, K. 1972 *Faraday Discuss. chem. Soc.* **54**, 257.

Helenelund, K. 1984 Post-collision interaction and vibrational excitations following core-hole creation and decay. Thesis. Acta Universitatis Upsaliensis no. 757.

Johansson, B. & Mårtensson, N. 1980 *Phys. Rev.* B **21**, 4427.

Larsson, N., Stenius, P., Eriksson, J. C., Maripuu, R. & Lindberg, B. 1982 *J. Colloid Interface Sci.* **90**, 127.

Lindberg, B., Maripuu, R., Siegbahn, K., Larsson, R., Gölander, C.-G. & Eriksson, J. C. 1982 *J. Colloid Interface Sci.* **95**, 308.

Lundholm, M., Siegbahn, H., Holmberg, S. & Arbman, M. 1985 *Uppsala Univ. Inst. Phys. Rep.* no. UUIP-1134.

Margaritondo, G. 1983 *Surf. Sci.* **132**, 469.

Maripuu, R. 1983 Electronic and molecular structure in molecules studied by u.v. and X-ray electron spectroscopy and e.s.c.a. investigations of heparinized and related surfaces. Thesis. Acta Universitatis Upsaliensis no. 696.

Mehlhorn, W. (ed.) 1982 *Handbuch der Physik*, vol. XXXI, Corpuscles and radiation in matter I. Heidelberg: Springer.

Nilsson, A., Mårtensson, N., Hedman, J., Eriksson, B., Bergman, R. & Gelius, U. 1985 Presented at the European Conf. on Surface Science (ECOSS-7) in Aix, France on 1–4 April 1985. Submitted for publication in *Surf. Sci.*)

Norell, K.-E., Baltzer, P., Wannberg, B. & Siegbahn, K. 1984*b* *Nucl. Instrum. Meth.* **227**, 499.

Norell, K.-E., Wannberg, B., Veenhuizen, H., Nohre, C., Karlsson, L., Mattsson, L. & Siegbahn, K. 1984*a* *Uppsala Univ. Inst. Phys. Rep.* no. UUIP-1109.

Poon, H. C. & Tong, S. Y. 1984 *Phys. Rev.* B **30**, 6211.

Price, W. C. & Turner, D. W. (eds) 1970 A Discussion on photoelectron spectroscopy. *Phil. Trans. R. Soc. Lond.* **A 268**.

Purtell, R., Hollinger, G., Rubloff, G. W. & Ho, P. S. 1983 *J. Vac. Sci. Technol.* **A1**, 566.

Robinson, H. 1925 *Phil. Mag.* **50**, 241.

Siegbahn, H. 1985 *J. phys. Chem.* **89**, 897.

Siegbahn, K., Gelius, U., Siegbahn, H. & Olson, E. 1970 *Phys. Lett.* A **32**, 221; also *Physica Scr.* **1**, 272.

Siegbahn, K., Hammond, D., Fellner-Feldegg, H. & Barnett, E. F. 1972 *Science, Wash.* **176**, 245.

Siegbahn, H., Lundholm, M., Holmberg, S. & Arbman, M. 1983 *Physica Scr.* **27**, 431.

Siegbahn, K., Nordling, C., Fahlman, A., Nordberg, R., Hamrin, K., Hedman, J., Johansson, G., Bergmark, T., Karlsson, S.-E., Lindgren, I. & Lindberg, B. 1967 E.s.c.a.: atomic, molecular and solid state structure studied by means of electron spectroscopy. *Nova Acta. Soc. Scient. upsal* Ser. IV, **20**.

PHILOSOPHICAL TRANSACTIONS OF THE ROYAL SOCIETY A MATHEMATICAL, PHYSICAL & ENGINEERING SCIENCES

Siegbahn, K., Nordling, C., Johansson, G., Hedman, J., Hedén, P. F., Hamrin, K., Gelius, U., Bergmark, T., Werme, L. O., Manne, R. & Baer, Y. 1969 *E.s.c.a. applied to free molecules*. Amsterdam: North-Holland.

Turner, D. W., Baker, C., Baker, A. D. & Brundle, C. R. 1970 *Molecular photoelectron spectroscopy*. London: Wiley-Interscience.

Veenhuizen, H., Wannberg, B., Mattsson, L., Norell, K. E., Nohre, C., Karlsson, L. & Siegbahn, K. 1984 *Uppsala Univ. Inst. Phys Rep.* no. UUIP-1107.

Waldrop, J. R., Kovalczyk, S. P. & Grant, R. W. 1982 *J. Vac. Sci. Technol.* **21**, 607.

Wannberg, B., Lee, T. K., Nordfors, D., Karlsson, L., Mattson, L. & Slegbahn, K. 1985 (In preparation.)

Wannberg, B., Veenhuizen, H., Mattsson, L., Norell, K.-E., Karlsson, L. & Siegbahn, K. 1984*a* *J. Phys.* **B 17**, L259.

Wannberg, B., Veenhuizen, H., Norell, K.-E., Karlsson, L., Mattsson, L. & Siegbahn, K. 1984*b* *Uppsala Univ. Inst. Phys. Rep.* no. UUIP-1110.

PHILOSOPHICAL TRANSACTIONS OF THE ROYAL SOCIETY A MATHEMATICAL, PHYSICAL & ENGINEERING SCIENCES